PRESSURE-DEPENDENT LINE PARAMETERS OF CO_2 BY MULTISPECTRUM LEAST-SQUARES FITTING

A project submitted in partial fulfillment of the requirements
for the degree of Bachelor of Science with a concentration in Physics
from the College of William and Mary

by

Gregory DiComo

Williamsburg, VA
April 2005

Abstract

High-resolution spectra of CO_2 in the 4700-4930 wavenumber region have been used to determine the α_l self-induced pressure-broadening coefficient and the δ self-induced pressure-shift coefficient for some 470 lines. These coefficients were determined using a multispectrum nonlinear least-squares fitting technique [1]. They have been determined for many of the lines in the 20013 ← 00001, 21113 ← 01101, 40002 ← 01101, and 22213 ← 02201 bands of $^{12}C^{16}O_2$, and the 20012 ← 00001 and 20013 ← 00001 bands of $^{13}C^{16}O_2$. Values for the two parameters have been found to range between 0.0551 and 0.1326 cm^{-1}/atmosphere for α_l, and between -0.0183 and 0.0192 cm^{-1}/atmosphere for δ. Errors for the two parameters have been found to range from 7.00E-05 to 2.60E-02 cm^{-1}/atmosphere for α_l, and from 1.20E-04 to 9.01E-03 cm^{-1}/atmosphere for δ. The constraint-based fitting technique has been shown to be of use for obtaining stable solutions, thus admitting the unconstraining of additional spectral line parameters. Pressure-broadening coefficients have been found to vary significantly between bands for lines of identical values of the quantum number |m|.

1 Introduction

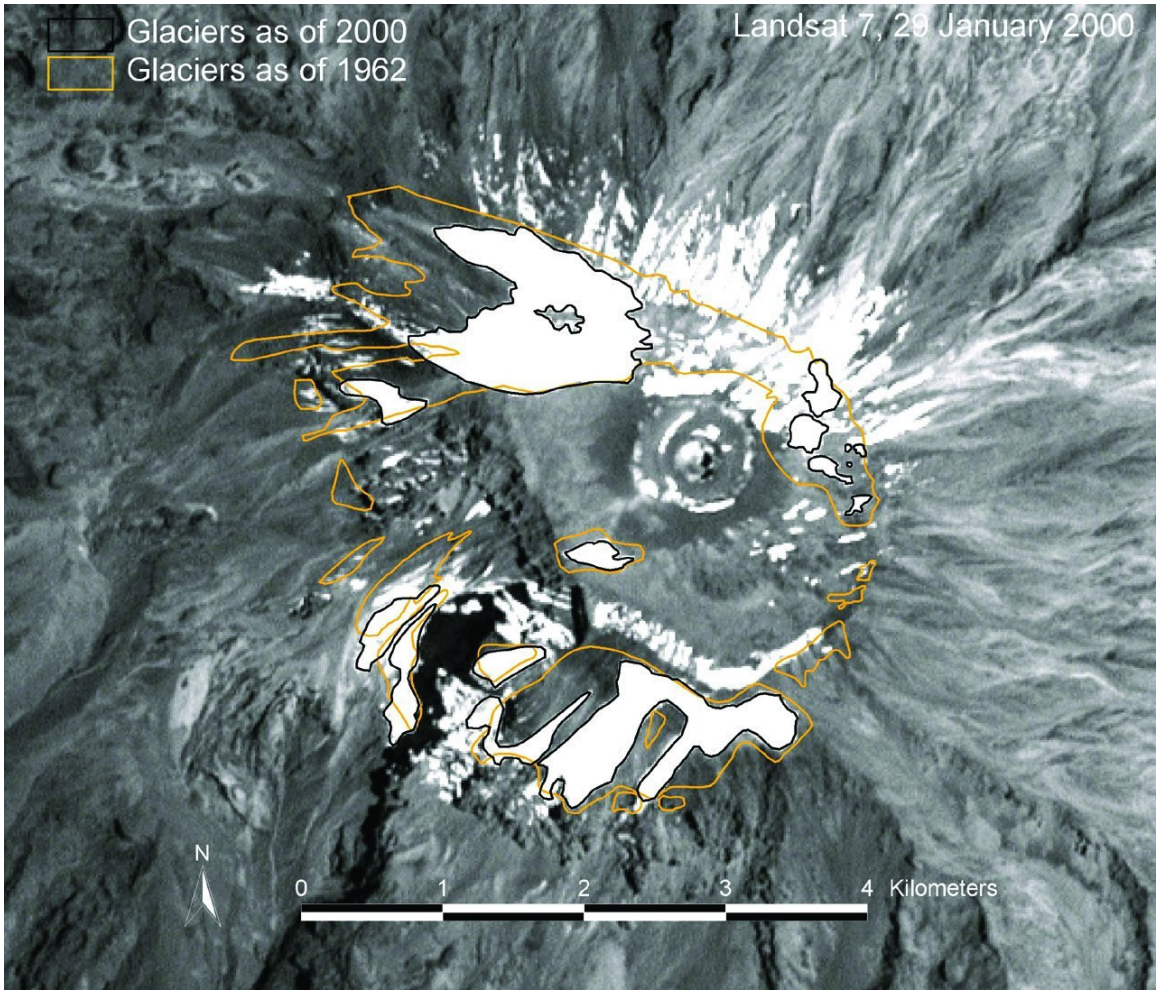

Fig. 1. A satellite photograph of the top of Mount Kilimanjaro, with outlines indicating the recession of glaciers between 1962 and 2000 [2].

Figure 1 is a satellite photograph of the top of Mount Kilimanjaro taken in January 2000 by Landsat 7 and Landsat 29. The orange outlines indicate the extent of glaciation on the mountain as of 1962, while the black outlines indicate the extent of glaciation as of January 2000. The decrease in glaciated area is dramatic. This photograph implies the operation of an ongoing process of rapid climate change during the latter half of the 20th century. While the photograph does not provide rigorous scientific evidence for climate change on a global scale, it and anecdotal evidence like it are sufficient to spur an investigation into the phenomenon, and what anthropogenic processes might drive it.

Carbon dioxide is the fifth most abundant molecule in the Earth's atmosphere, behind nitrogen, oxygen, water, and argon. It is the second most active absorber of infrared light in the atmosphere, next to water vapor, and since 1750 its concentration has risen from approximately 280 parts per million to approximately 370, an increase of 32% [3]. Because of its ability to absorb infrared light and its dramatic increase in concentration since the industrial revolution, carbon dioxide has been identified as the

most important anthropogenic source of climate change [3]. As such, precise measurement of CO_2 concentrations over wide areas is important for the study and prediction of climate change [3].

The usual technique for determining the composition of such large volumes of gas is remote sensing by spectroscopy: the atmosphere's spectrum is compared to the known spectra of the gasses which it is expected to contain and decomposed into a sum of those spectra [4]. O'Brien, Rayner, *et al* demonstrated that remote sensing projects such as the Orbiting Carbon Observatory [5] must be able to determine the concentration of CO_2 in a vertical column of air with a precision of one part in 370 or better in order to tell the difference between CO_2 sources and sinks on a large scale [6,7]. This is naturally impossible without a thorough knowledge of carbon dioxide's spectrum, including line parameters such as position, intensity, and pressure broadening and pressure shift coefficients [4]. Yang *et al* found that in order to attain the desired precision in measurement of columnar CO_2 concentrations, the underlying spectral line parameters would have to be determined to a precision of approx. 0.5% – far greater than that given in the 2000 HITRAN database of spectral parameters [8,9].

Precise determination of the spectral line parameters of CO_2 is possible by using data regression techniques to fit experimentally obtained spectra [10,11]. A theoretical spectrum is computed based on known spectral line parameters. Numerical iterations are performed on some or all of those parameters in order to minimize the sum of the squares of the differences between a single experimentally obtained spectrum and the calculated spectrum. Thus, the precision with which those parameters are known is improved. In 1995 Benner *et al* introduced a computer program written in FORTRAN which iterates on numerical solutions for individual line parameters to fit multiple spectra simultaneously [1]. It also allows the introduction of equations constraining the values of some parameters to functions of others. When line parameters are constrained to their theoretically determined values as functions of the underlying properties of the molecule, the program iterates on the underlying parameters, thus determining them with great precision. Furthermore, the decrease in the number of unconstrained parameters leads to a decreased likelihood of the solution iterating to divergence, and increased ability to unconstrain additional parameters without disrupting the solution. This constraint-based multispectrum least-squares fitting technique allows the introduction of multiple spectra to corroborate the parameter values and decrease the standard error.

In this experiment, these data analysis techniques have been applied to eleven spectra in order to determine the self-induced pressure broadening coefficients (α_l) and self-induced pressure shift coefficients (δ) for many of the spectral lines in the 4500-4930 wavenumber region of carbon dioxide.

2 Physics Background

Carbon dioxide is a linear triatomic molecule, with its two oxygen atoms on either side of the carbon atom on the Z-axis. As such, it has four rovibrational modes: X-axis or Y-axis spinning (indistinguishable by symmetry), symmetric stretching, asymmetric stretching, and a doubly degenerate bending state. The molecule may also possess angular momentum along the Z-axis, but only when the bending state is excited. Each mode can store discrete amounts of energy in a series of states analogous to that of a particle in a potential well. The energy states admitted by the electron clouds of the individual atoms are large compared to those of the molecule itself; however, transitions between those states lead to lines in the ultraviolet spectrum, and therefore they are not considered.

Each absorption line in the spectrum corresponds directly to a transition from one of these allowed energy states of one of the rovibrational modes to a higher energy state as the molecule absorbs a photon of the appropriate energy. The line's position, ω, (that is, its wavenumber in cm^{-1}) is related to this energy:

$$\omega = (1 / \lambda) = (E / (h c)) \qquad (1)$$

where λ is the photon's wavelength, E is its energy (equal to the difference in energy from the higher energy state to the lower energy state), h is Planck's constant, and c is the speed of light.

The position of any given line is shifted due to the collision of molecules in the sample with one another, and thus is linearly dependent on pressure:

$$\nu = \nu_0 + \delta p \qquad (2)$$

where ν_0 is the position of the line at zero pressure, p is the pressure of the sample which produced the spectrum in question, and the multiplicative constant δ is the self-induced pressure shift coefficient, measured in cm^{-1}/atmosphere. The parameter δ and all such spectral line parameters vary from line to line [12].

Because each line corresponds to a transition from one energy state to another, at a basic level of theory each line has a discrete position determined by the difference in those two energy states; that is, it has no width. However, in practice spectral lines have width produced by three main effects: the natural line profile, the Doppler line profile, and the Lorentz line profile.

The transmission of the gas is related to the line shape in the following manner:

$$T = e^{(-a S K_\omega)} \qquad (3)$$

where a is the amount of gas in the path, S is the natural intensity of the line as a function of temperature, and $K\omega$ is the line shape function. The line shape function is normalized to keep the area under the curve of the line after the application of the function equal to the area under the line before the application of the function. That is,

$$1 = \int_0^\infty K\omega \, d\omega \tag{4}$$

Thus, any line which gains width due to one of the following effects loses intensity in proportion [12].

The natural line shape (or natural dampening) is a broadening of the line due to the finite amount of time it takes the molecule to absorb energy. The effect is very small compared to the other two effects and is not of interest here.

The Doppler line shape ($K\omega_D$) is an overall broadening of the line due to the Doppler shift of molecules in the sample moving relative to the observer. Thus, it is a function of temperature:

$$K\omega_D = K\, e^{(-(\omega - \omega_0)^2 / (\alpha_D)^2)} \tag{5}$$

where ω is wavenumber in cm^{-1}, ω_0 is the center of the band in cm^{-1}, and α_D is the Doppler width coefficient [12]. The quantity K is well-established by theory:

$$K = (\omega / \alpha_D) \sqrt{(T / M)} \tag{6}$$

where T is the temperature of the sample in Kelvins, M is its molecular mass in Atomic Mass Units, ω is wavenumber in cm^{-1}, and α_D is the Doppler width coefficient [12]. Because the nature and workings of this process are already well-known from theory and experiment, and because the effect is small compared to the Lorentz line shape, it does not concern us further here.

The Lorentz line shape ($K\omega_L$) is a broadening of the line, especially near its base, due to collisions between the molecules in the sample. Thus, it is a function of temperature and pressure:

$$K\omega_L = K(\alpha_L) / ((\omega - \omega_0)^2 + \alpha_L^2) \tag{7}$$

where ω and ω_0 are defined as above, and the Lorentz broadening coefficient α_L contains the temperature and pressure dependence:

$$\alpha_L = \alpha_l (P / P_0) (T_0 / T)^n \tag{8}$$

where T and P are the temperature and pressure of the sample, T_0 is 296K, P_0 is one atmosphere, n is the line's temperature dependence exponent, and α_l is the pressure-dependent self broadening coefficient, measured in cm^{-1}/atmosphere [12]. Because the spectra used in this project were all taken at room temperature, values of n could not be determined. This project used values of n taken from the 2000 HITRAN line list [9].

In addition to the line-broadening effects discussed above, the finite physical nature of the real interferometer in an FTS (Fourier Transform Spectrometer) produces two additional broadening effects $O(\sigma)$: that due to finite maximum path difference, and that due to finite entrance aperture size.

The finite maximum path difference of the interferometer introduces a sinc function that convolutes the spectrum:

$$O_{path}(\sigma) = 2\,L\,\mathrm{sinc}\,(\,2\,L\,\sigma\,) \qquad (9)$$

where L is the maximum path difference of the interferometer and σ is the wavenumber in cm^{-1} [13]. The sinc function introduces a "ringing" effect around each line which can cause the observed line to display absorption greater than 100% at its center, and lower than 0% at the edges. This effect is strictly a nonphysical artifact of FTS design.

The finite entrance aperture for the light introduces a rectangular function that convolutes the spectrum:

$$O_{aperture}(\sigma) = (\,(\,2\,\pi\,)\,/\,\sigma_0\,)\,\Pi\,(\,(\,2\,\pi\,\sigma\,)\,/\,(\,\sigma_0\,\Omega_m\,)\,) \qquad (10)$$

where σ_0 is the linecenter, Π is the rectangular function with width equal to the inverse of the coefficient of the variable σ within its argument, and Ω_m is the solid angle from the center of the collimating lens to the edge of the aperture [13]. The rectangular function has a width $\mathbf{w = \sigma_0\Omega_m\,/\,2\pi}$ and serves to broaden each line while keeping the area constant. A well-chosen aperture size can all but eliminate this effect [13].

The product of these two functions is known as the instrumental function. Because the parameters of the instrumental function are well-known for the spectrometer used in this experiment, and because the fitting program used in this study corrects for them, these effects do not concern us further here [1].

The spectrum itself is never measured directly by the FTS detectors – rather, they measure a plot of intensity versus path difference called an interferogram, which is then transformed into the spectrum via an inverse Fourier transform. The orthogonality of the sine and cosine functions guarantees that any periodic function of any variable can be expressed as the linear combination of an infinite series of sine and cosine functions of various amplitudes. The inverse Fourier transform is an operation which, given any periodic function of any variable ($f(x)$), outputs a new function ($F(\sigma)$) which represents a plot of the amplitudes of the sinusoid functions which compose it, as a function of their frequencies. It is defined as

$$F(\sigma) = \int_{-\infty}^{\infty} f(x)\, e^{(\,2\,i\,\pi\,\sigma\,x\,)}\, dx \qquad (11)$$

where F is the inverse Fourier transform of f, and i is the square root of negative one. The interferogram measured by This transformation will yield a complex function for any but a perfectly symmetric interferogram. The imaginary part of the spectrum can be interpreted as a phase term to be applied to the real part of the spectrum, where the phase

is equal to the arctangent of the ratio of the imaginary and real parts [13]. This phase correction is often carried out before data analysis begins.

Because the electronics which record the interferogram are digital mechanisms with a finite sampling rate, the discrete Fourier transform must be used:

$$F(\sigma_k) = (1/N) * \sum_{j=1}^{N} (f(x_j) * e^{(-2 i \pi \sigma x_j)}) \qquad (12)$$

where N is the number of data points in the interferogram [13]. This function transforms a series of N discrete measurements of intensity as a function of path difference into N complex numbers as a function of frequency.

In this project spectral bands are labeled by two sets of quantum numbers indicating which vibrational transition produces the band. The sets are organized with the higher energy of the two states on the left, and the lower on the right; they are joined by a left-pointing arrow to indicate that the molecule absorbs energy and transitions from a low-energy state to a higher one. These band-identifying number sets are a series of five numbers based on the vibrational quantum numbers for CO_2:

$$v_1 v_2 \ell v_3 \; r \qquad (13)$$

where v_1 is the excitation state of the symmetric vibration mode, v_2 is the excitation state of the bending mode, ℓ is the excitation state of the angular momentum due to bending, v_3 is the excitation state of the asymmetric vibration mode, and r is the Fermi resonance ranking index. Parameters v_1, v_2, and v_3 are truly independent and can take any integer value, while ℓ is always the same as v_2, and r is restricted to values ranging from $v_1 + 1$ down to one in integer steps. The Fermi resonance r is an index chosen to break the degeneracy resulting from the coincidental near equivalence in energy between an excitation in v_1 and double the excitation in v_2. It decreases with increasing energy [9].

The positions and intensities for the lines in several vibrational bands fitted in this project have been constrained to functions of underlying band parameters. For positions, those band parameters are (G'-G"), the bandcenter, B' and B", the rotational constants of the upper and lower states, D' and D", the centrifugal distortion constants of the upper and lower states, and H' and H", the second-order distortion coefficients of the upper and lower states [14]. Each of these parameters varies from band to band and is measured in units of cm^{-1}. Throughout this paper the superscript ' refers to a parameter of the upper vibrational state that produces the band, while the superscript " refers to a parameter of the lower vibrational state. For intensities, the parameters are A_1, A_2, and A_3 – the "*F*-factor" coefficients. It is useful for brevity to define the rotational energies:

$$E"_{rot} \equiv (J"(J"+1))(B"-(J"(J"+1))(D"-(J"(J"+1)H")) \qquad (14)$$

and

$$E'_{rot} \equiv (J'(J'+1))(B'-(J'(J'+1))(D'-(J'(J'+1)H')) \quad (15)$$

where J is the line's rotational state quantum number. These quantities are measured in units of cm^{-1}. It is also worth noting that J' is always equal to $J''-1$ for the P branch of any band, while it is always equal to $J''+1$ for the R branch. Therefore, line lists customarily index lines by their branch and value of J''.

For lines in noninteracting bands which have been constrained to functions, the line positions ν are constrained to:

$$\nu = (G'-G'') + E'_{rot} - E''_{rot} \quad (16)$$

where all parameters are as defined above [14]. Note that E'_{rot} and E''_{rot} contain dependence on J''.

For lines in noninteracting bands which have been constrained to functions, the line intensities S are constrained to:

$$S = ((S_{\nu} L_i \nu) / ((G'-G'') Q_r)) (F) e^{(-C_2 / T_0) E''} \quad (17)$$

where S_{ν} is the vibrational band intensity, ν is the line's position, Q_r is the lower state rotational partition function at 296K, C_2 is the second radiation constant, T_0 is 296K, E'' is the line's lower-state energy (distinct from E''_{rot}), and L_i is the Hönl-London factor, equal in this case to the absolute value of m. The quantum number m is defined as $-J''$ for the P branch and $J''+1$ for the R branch [14]. No Q branches are treated in this work. The coefficient F – the *F*-factor – contains a dependence on three additional coefficients:

$$F = (((A_3 m + A_2) m + A_1) m + 1)^2 \quad (18)$$

where all parameters are as defined above [14]. Note that S is dependent on J'' both inside and outside the coefficient F.

For the interacting band 40002 ← 01101 the position constraint equations are not so simple. The positions of lines in that band, as well as its interacting band – those lines of 21113 ← 01101 with odd values of J'' – have been constrained to:

$$\nu = (1/2) (E'_{21113} + E'_{40002}) \pm \sqrt{(E'_{21113} + E'_{40002})^2 - 4 (E'_{21113} E'_{40002} - \omega^2 J'(J'+1))} \quad (19)$$

where ω is the perturbation constant for the two interacting bands, and $E_{v1\ v2\ \ell\ v3\ r}$ is defined as $(E'_{rot} + (G'-G''))$ for the upper level indicated in the subscript and the lower level which the two interacting bands share.

Uncertainties ε_A for parameters constrained to equations in this manner may be derived through use of the formula

$$\begin{aligned}\varepsilon_A^2 = &((\partial A/\partial B) \varepsilon_B)^2 + ((\partial A/\partial C) \varepsilon_C)^2 \\ &+ ((\partial A/\partial D) \varepsilon_D)^2 + \ldots + \rho_{BC} (\partial A/\partial B) (\partial A/\partial C) \varepsilon_B \varepsilon_C \\ &+ \rho_{BD} (\partial A/\partial B) (\partial A/\partial D) \varepsilon_B \varepsilon_D + \ldots\end{aligned} \qquad (20)$$

where ε_A is the uncertainty in the parameter which is constrained to a function, ε_B through ε_D and beyond are the uncertainties in any unconstrained parameters which appear in the function, $(\partial A/\partial B)$ is the partial derivative of the parameter which is constrained to the function with respect to each unconstrained parameter, and ρ_{BC} is the correlation between unconstrained parameters B and C which both appear in the same equation [1]. Correlation coefficients are generated as part of the least-squares fit.

3 Experimental Method

All eleven spectra for this project were taken at the 1-meter Fourier Transform Spectrometer (FTS) at the McMath-Pierce Solar Telescope at Kitt Peak National Observatory in Tucson, Arizona. For these spectra the spectrometer was configured using two liquid nitrogen-cooled Indium Antimonide Diode detectors and a Gallium Phosphide-coated Calcium Fluoride beam splitter. The samples of CO_2 were pumped into a 6-meter White multi-pass absorption cell mounted on the wall of the facility. For spectra 8 through 11 the White cell was wrapped in a layer of electric blankets followed by a layer of aluminum-coated plastic insulation in an attempt to stabilize temperature variations across its length; initial experimentation with this system proved it ineffective, and the blankets were left unplugged for the duration of the runs. A bright Halogen source with quartz windows, white in the infrared, was set up pointing into the White cell. The light output from the White cell was reflected through a series of hollow plastic tubes and boxes to point directly into the spectrometer's input. The system of tubes could not practically be evacuated; therefore, it was purged with dry nitrogen recently evaporated from the liquid state in order to reduce the amount of water in that portion of the path. This system, approximately two meters in length, was noted as a potential source of systematic error, as it could still contain gasses such as water, nitrogen, and atmospheric CO_2.

This configuration enabled the recording of spectra in the range of 3500-7500 cm^{-1} with a resolution of 0.012 cm^{-1} for spectra 1 through 7, and 0.013 cm^{-1} for spectra 8 through 11. The data for this project consist of the 4700-4930 cm^{-1} segment of these larger spectra. A brief description of the workings of the FTS and White multi-pass absorption cell follows.

A Fourier Transform Spectrometer is a multiplex instrument in which the intensity distribution of a spectrum is recorded simultaneously at all frequencies [13]. Light from the source enters the instrument through an aperture, is collimated, and encounters a Michelson interferometer. The light is split into two paths of slightly different length, recombined, and reflected onto a detector. The mirror at one end of one of the optical paths moves smoothly back and forth in order to change the length of that path. As the movable mirror makes a pass from one end of its travel to the other, the detector samples the light at regular intervals in order to record an interferogram – a measurement of the light's intensity as a function of difference in length between one path and the other. Multiple passes are made in order to reduce the noise level of the interferogram. An inverse Fourier transform is performed on the resulting data, yielding a plot of the light's intensity as a function of frequency – a spectrum. The spectral region measured depends on the detectors and light filters used in the interferometer, and the resolution of the spectrum in the infrared is inversely proportional to twice the maximum path difference.

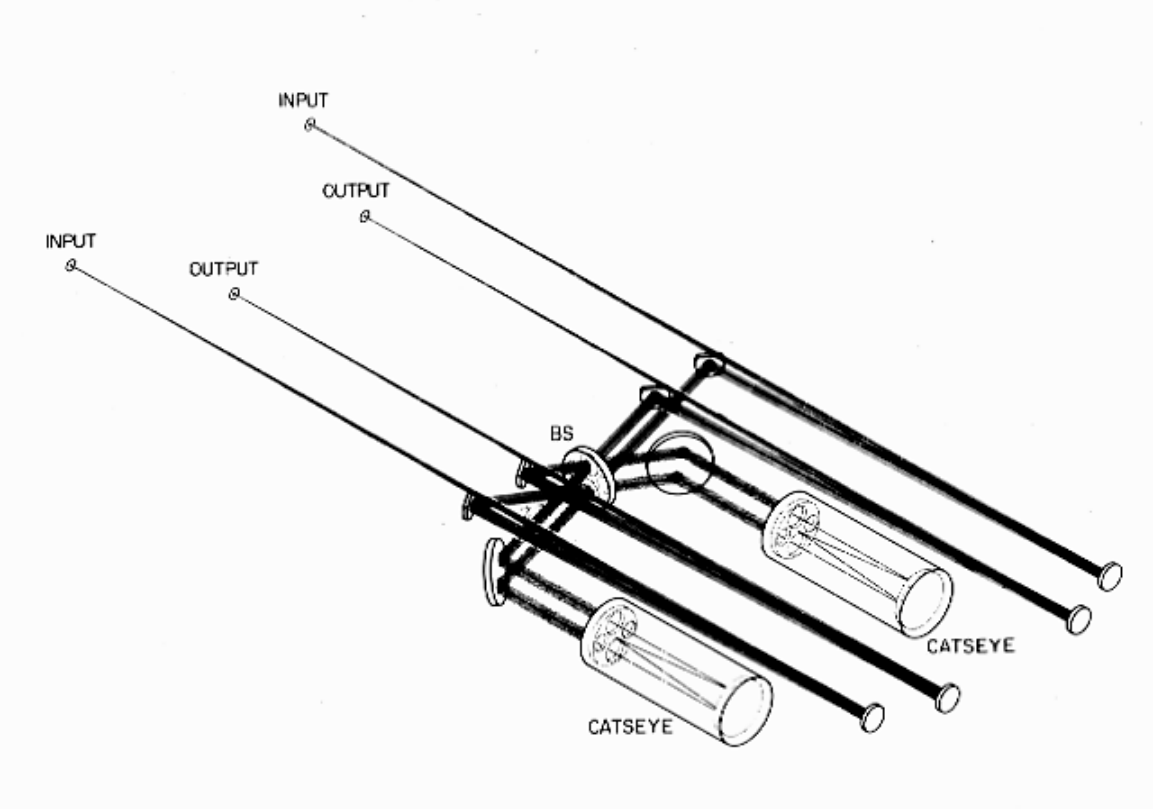

Fig. 2. A schematic diagram of the optics of the 1-meter FTS at the McMath-Pierce Solar Telescope at Kitt Peak National Observatory in Tucson, AZ [15].

The Kitt Peak FTS is a folded Michelson interferometer in a vacuum chamber. During operation, the vacuum ranges from 10^{-2} to 10^{-1} Torr. Although the FTS has two input apertures, in practice only one is used. It is 8 mm in diameter. The optics are set up in such a way that no light returns to the input – see Figure 2. The light that would return to the input in an unfolded Michelson interferometer is instead routed to a second detector so that no light is lost [15]. Each detector records a slightly different intensity distribution – since the light outputs have complementary phases, the difference of their signals is recorded as the interferogram.

Spectrum 1 and spectra 8 through 11 were taken using samples contained in a White multi-pass absorption cell, which reflects the light multiple times through a single column of gas, thus greatly increasing the path length without increasing the size of the instrument. A White cell consists of a sealed cylindrical metal chamber, insulated from temperature fluctuations, into which gas can be pumped through a series of valves. It has two windows in one end: one for light input, and one for output. At either end of the cell are mounted a series of mirrors. See Figure 3.

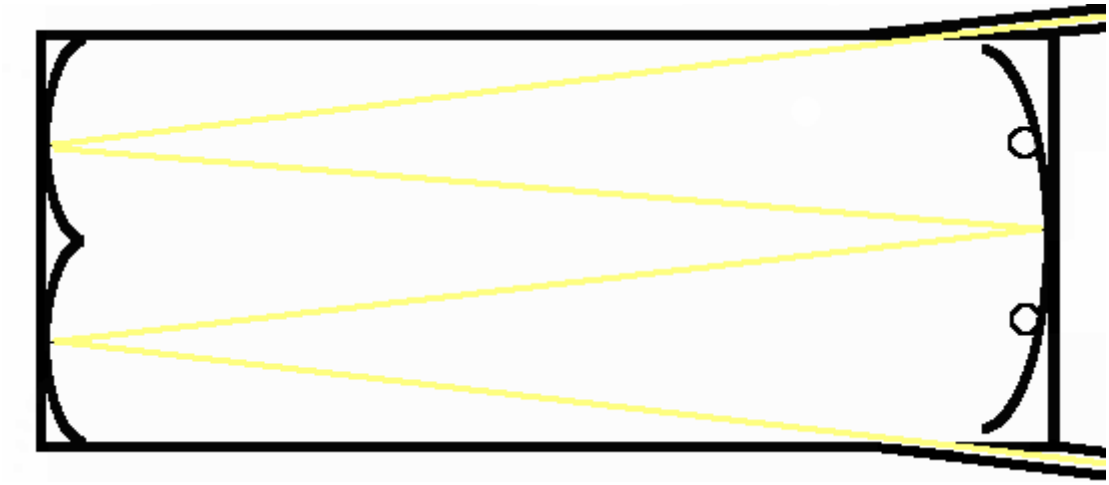

Fig. 3. A schematic diagram of a White style multipass absorption cell. The minimum possible path length is illustrated. For longer path lengths, the mirrors at the left are adjusted to reflect the beam of light roughly onto the points marked with circles on the large mirror, thus increasing the number of times the beam reflects before escaping the chamber. Figure not to scale [16].

These mirrors are arranged in such a way that the light from the input port falls on the first far mirror and is repeatedly reflected between that and a single focal point on the large near mirror. The light fills the first far mirror and then crosses the cusp onto the second far mirror, which causes it to begin reflecting onto a second focal point on the large near mirror. After a number of passes through the cell (adjustable by means of tilting the small far mirrors), the light falls off the edge of the near mirror and exits the cell through the output port. The repeated use of individual focal points on the large mirror ensures that the image of any debris on the mirrors will always fall on the debris itself, preventing the error from propagating and decreasing the amount of intensity lost compared to setups which use more optical components. In this way, long or short path lengths can be selected simply by means of adjusting the mirrors [16].

The six-meter base-path-length White cell at the Kitt Peak FTS has a total volume of approximately 600 liters, and an externally adjustable path length ranging from 24 to 432 meters in increments of 24m [15]. It was configured for a variety of different path lengths and pressures, as summarized in the spectrum information below. The pressures of the samples were monitored using three Baratron model 220-B capacitance manometer heads with ranges of 0-10, 0-100, and 0-1000 Torr respectively, resolutions of 0.01% of their full scale ranges, and accuracies of ±0.15% of the reading.

4 Data Collection and Analysis

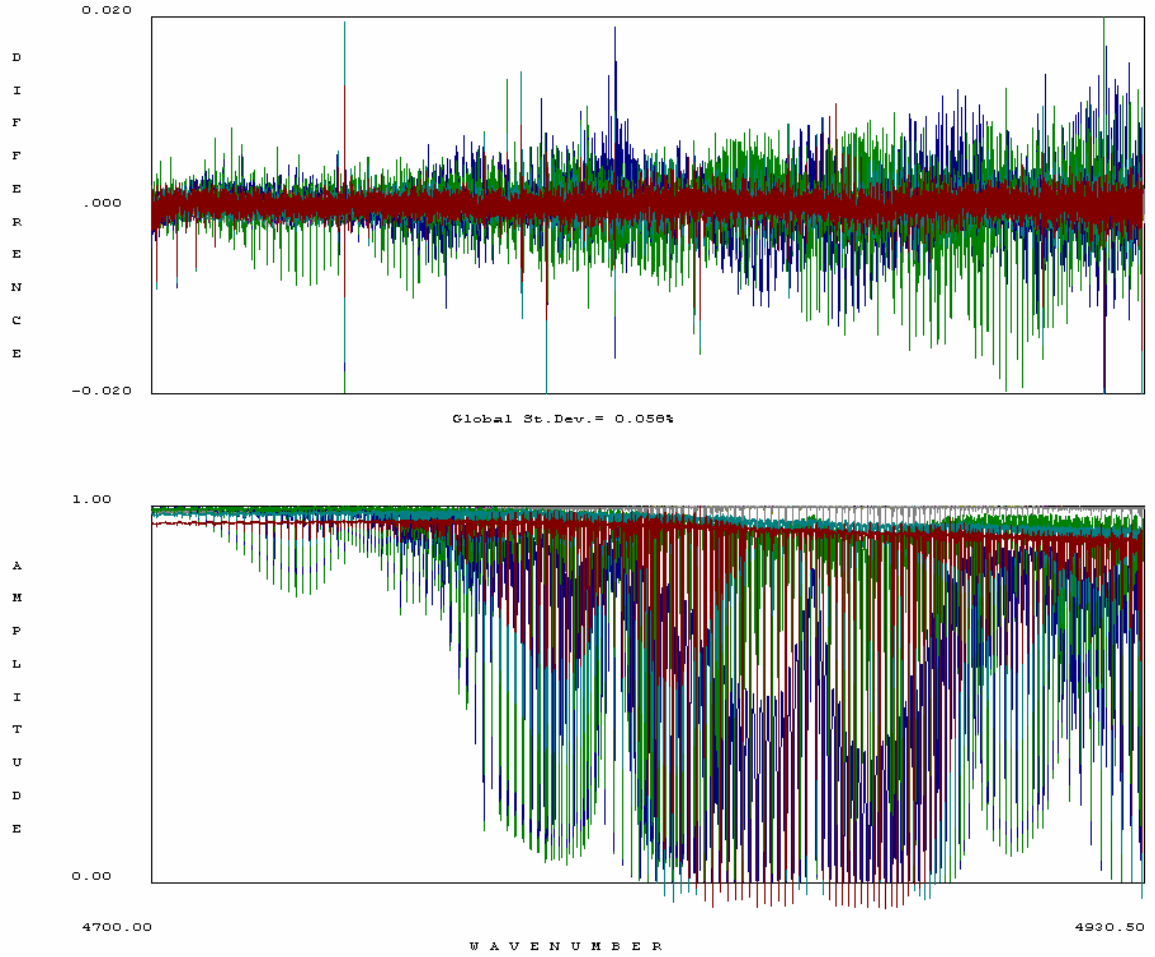

Fig. 4. Lower panel: overplot of all eleven spectra, with amplitude on the y-axis and wavenumber in cm^{-1} on the x-axis. The amplitude is the transmission offset by the zero level of the spectrum. Upper panel: expanded plot of the spectra's fit residuals.

Figure 4 is a color-coded overplot of all eleven spectra in the solution, and their residuals. This figure demonstrates the general shape of the bands and residuals, highlighting the locations of deficiencies in the fit. Note that the residuals are confined to ±0.020. Due to the large number of spectra, identifying any individual spectrum is difficult – therefore, they are presented individually on the following pages.

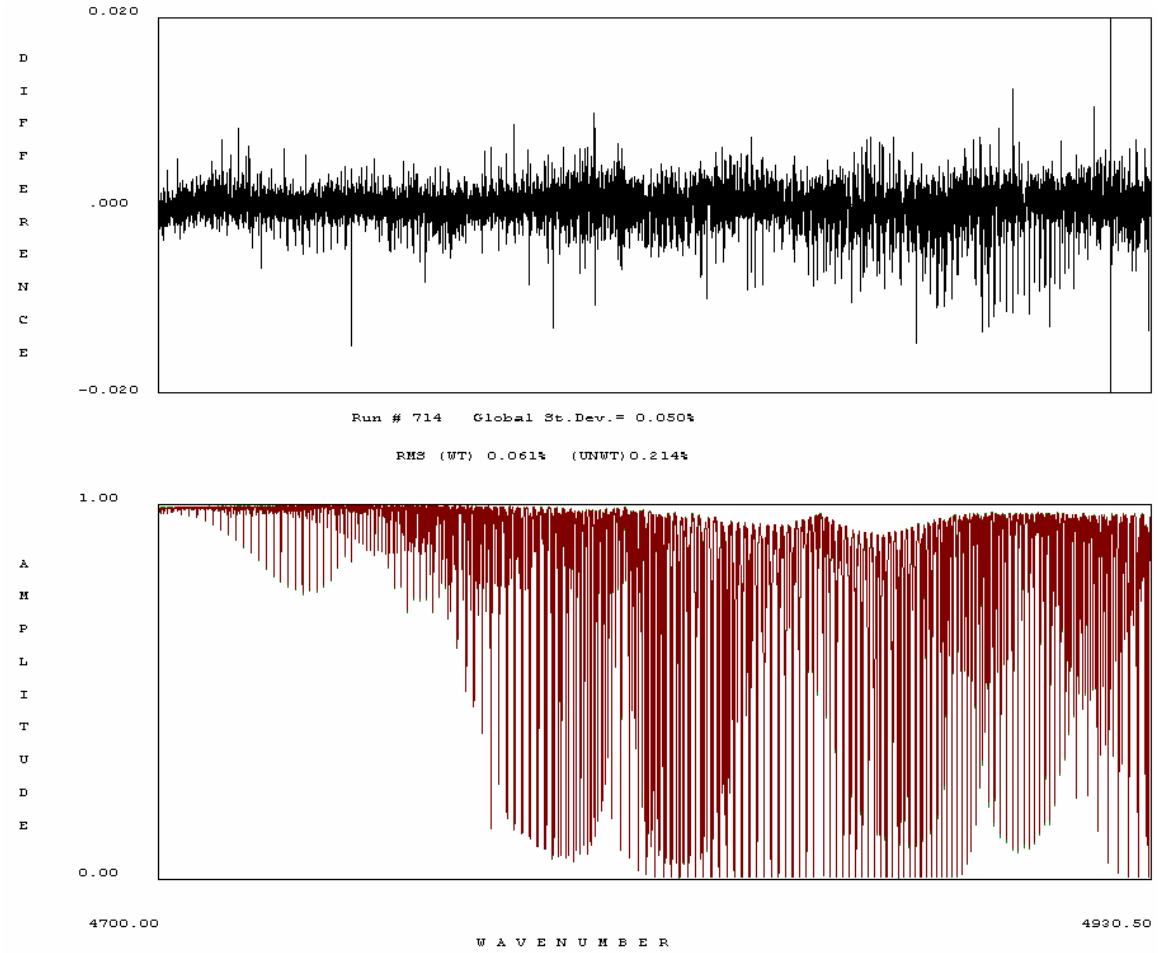

Fig. 5. Lower panel: spectrum 1 (green) and its fit (red), with amplitude on the y-axis and wavenumber in cm^{-1} on the x-axis. Note its low signal-to-noise ratio, the large number of bands visible, and the overall strength of the spectral lines, with many saturated (at 100% absorption). Upper panel: residuals of the fit.

Figure 5 depicts spectrum 1, the first of the spectra used in this investigation. It was taken for Dr. Lawrence Giver in 1995 by Dr. Linda Brown at Kitt Peak National Observatory, Arizona, on the Fourier transform infrared spectrometer (FTS) in the McMath-Pierce Solar Telescope. The spectrum was donated to this project in 2003. The sample in this case was a 6 meter base path length White cell filled with 79 Torr of pure CO_2, at a temperature of 24.25 degrees C. Its path length is 48.92 m, and the maximum path difference of the spectrometer was 49.057 cm. In many ways this spectrum is far from ideal. It is entirely saturated at many points, making precise identification of the relative strengths of the strongest lines difficult at best. Furthermore, the sample suffered some contamination by water of approximately .0035% - not enough to ruin the spectrum, but enough to introduce water lines. However, the strength of the lines in this spectrum makes it useful for identifying even weak CO_2 lines and constraining their positions to functions. Furthermore, the strong, well-known water lines in the spectrum are useful for wavenumber calibration. The phase correction applied by the FTS when this spectrum was taken led to residual phase errors – therefore, this spectrum's phase has been adjusted by 0.0048 degrees. The positions and intensities of the most significant lines in

this spectrum have already been determined through the function constraint technique. Approximately half of that work was done by myself; the other half was done by Emily Nugent. This spectrum forms a base on which the remaining ten spectra build. With the addition of those spectra, this one's weighting in the solution has been decreased to .0444.

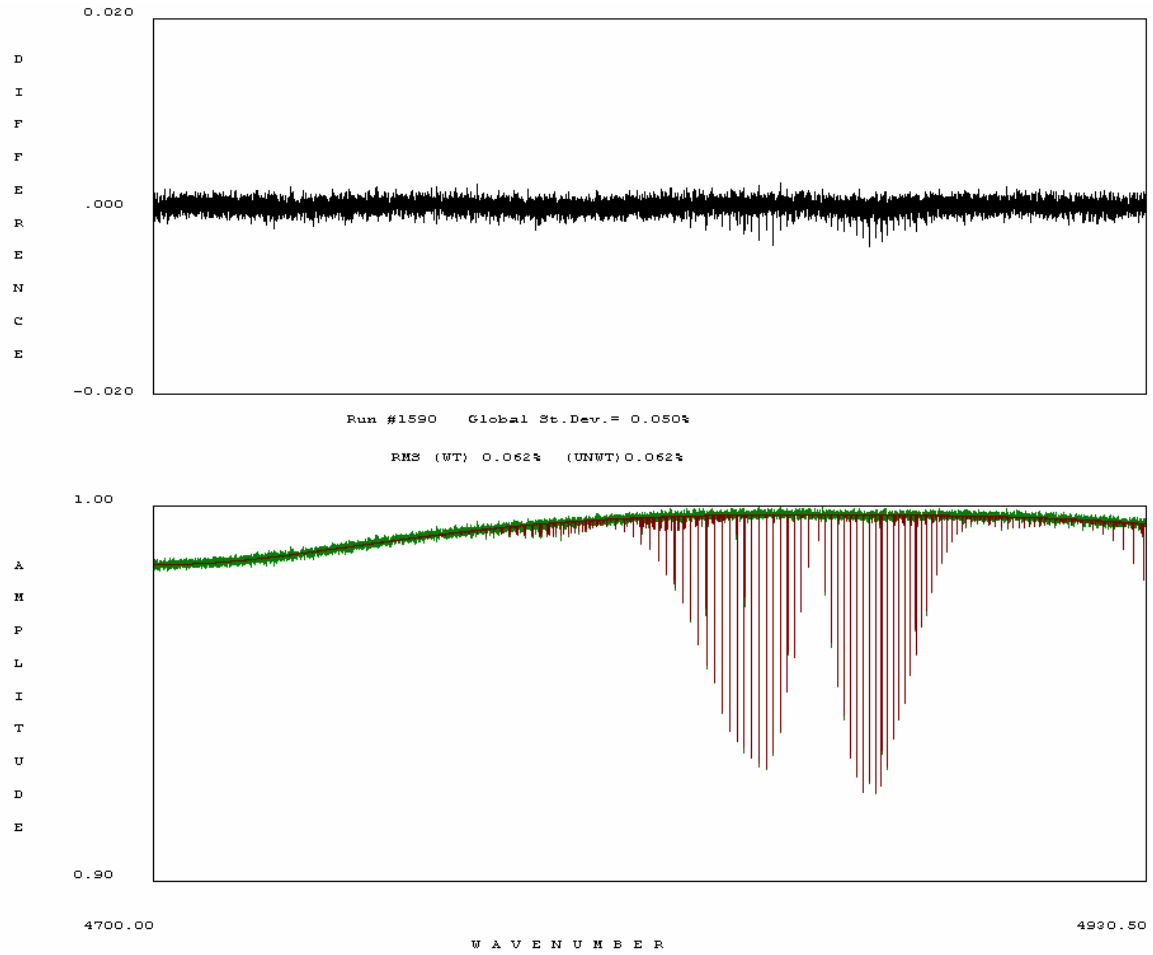

Fig.6. Lower panel: spectrum 2 (green) and its fit (red), with amplitude on the y-axis and wavenumber in cm^{-1} on the x-axis. Upper panel: residuals of the fit.

Figure 6 depicts spectrum 2. Spectra 2 through 7 were taken by Dr. Brown in 1997 at the Kitt Peak FTS. All of the 1590-1595 series spectra were recorded with a maximum path difference of 43.149 cm. Note the relatively sparse distribution of spectral lines, and one prominent band. For these reasons, spectra 2 through 7 are relatively simple to analyze. The sample was .101 meters of CO_2, at 29.93 Torr and 22.40 degrees C. Its current weighting in the solution is 1.00.

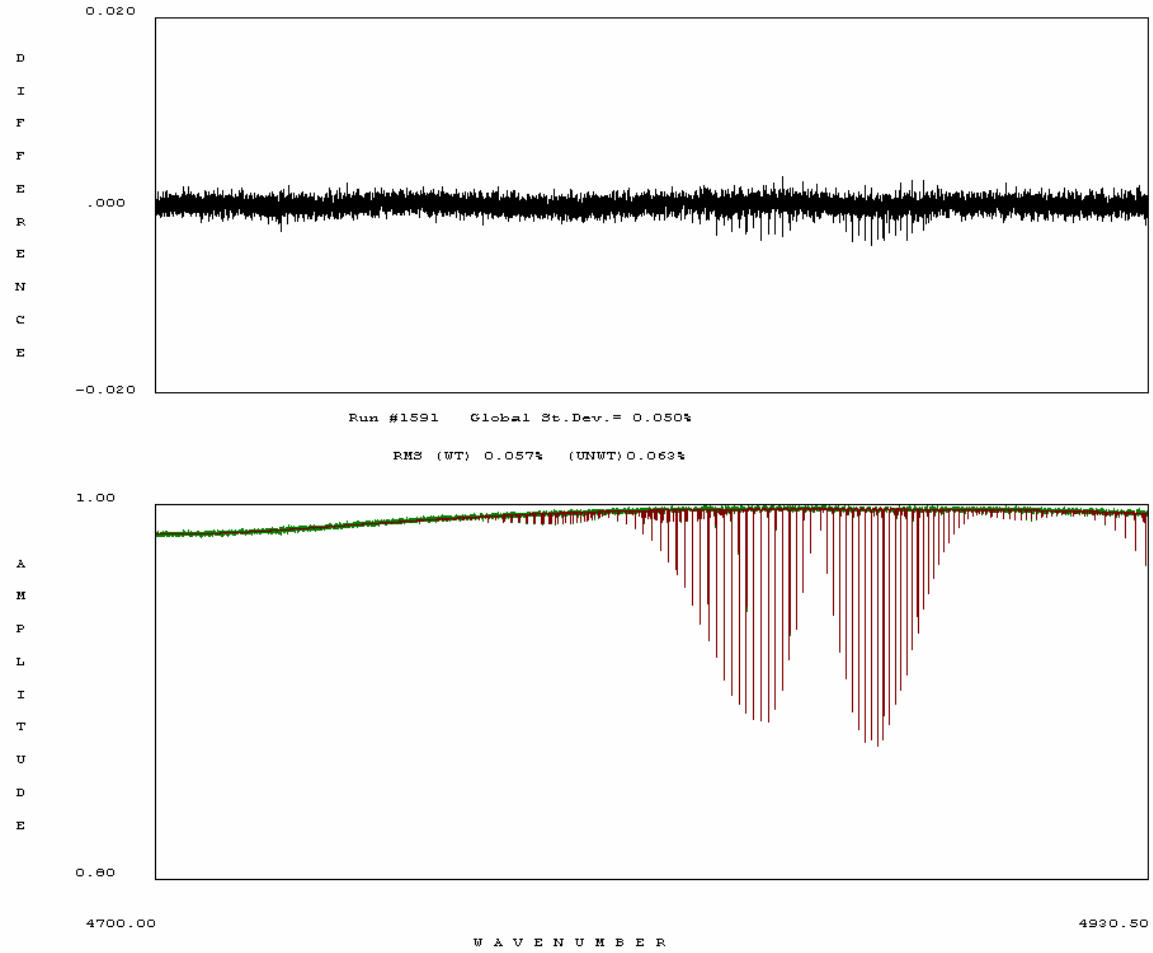

Fig. 7. Lower panel: spectrum 3 (green) and its fit (red), with amplitude on the y-axis and wavenumber in cm^{-1} on the x-axis. Upper panel: residuals of the fit.

Figure 7 depicts spectrum 3. The sample was .101 meters of CO_2, at 70.2 Torr and 22.70 degrees C. Its current weighting in the solution is 0.833.

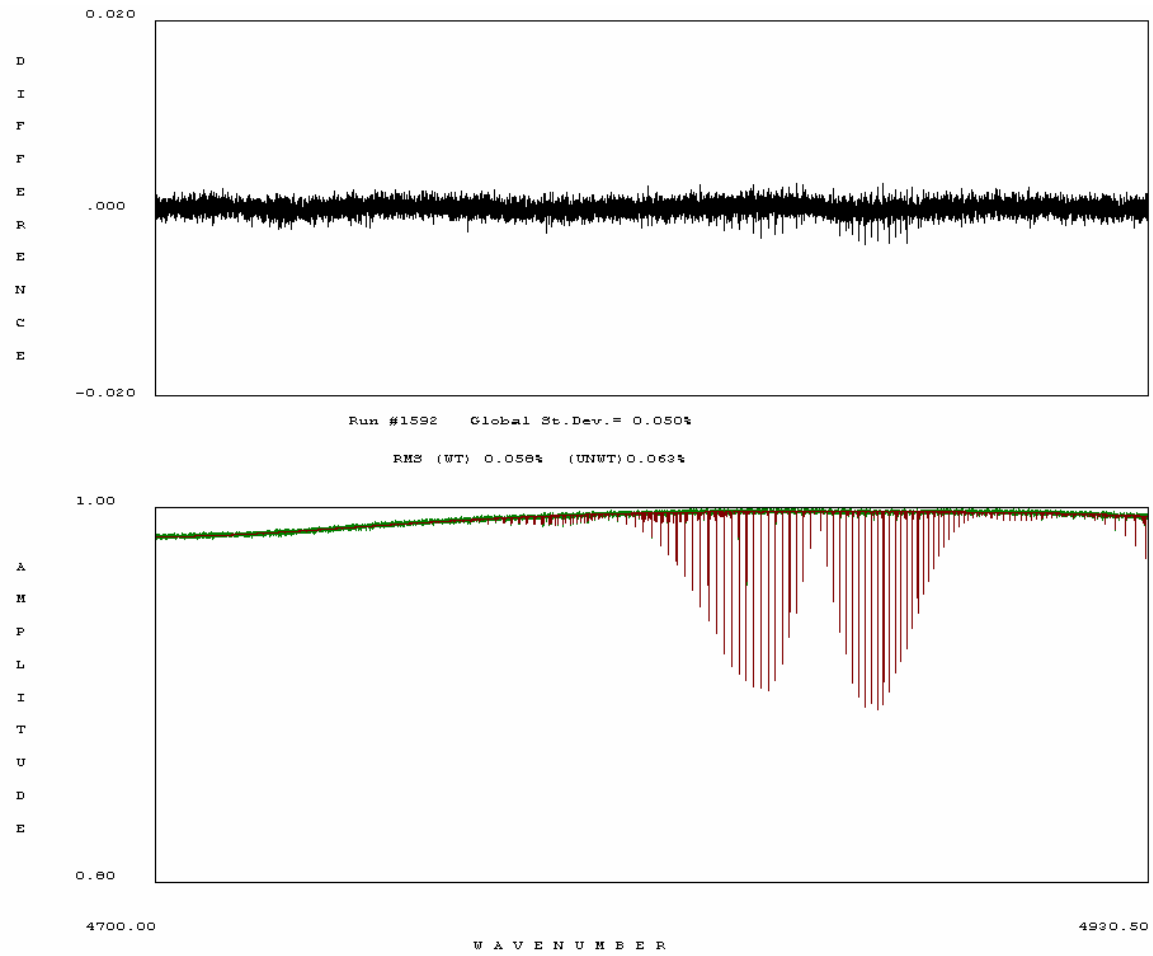

Fig. 8, Lower panel: spectrum 4 (green) and its fit (red), with amplitude on the y-axis and wavenumber in cm^{-1} on the x-axis. Upper panel: residuals of the fit.

Figure 8 depicts spectrum 4. The sample was .101 meters of CO_2, at 49.9 Torr and 23.00 degrees C. Its current weighting in the solution is 0.866.

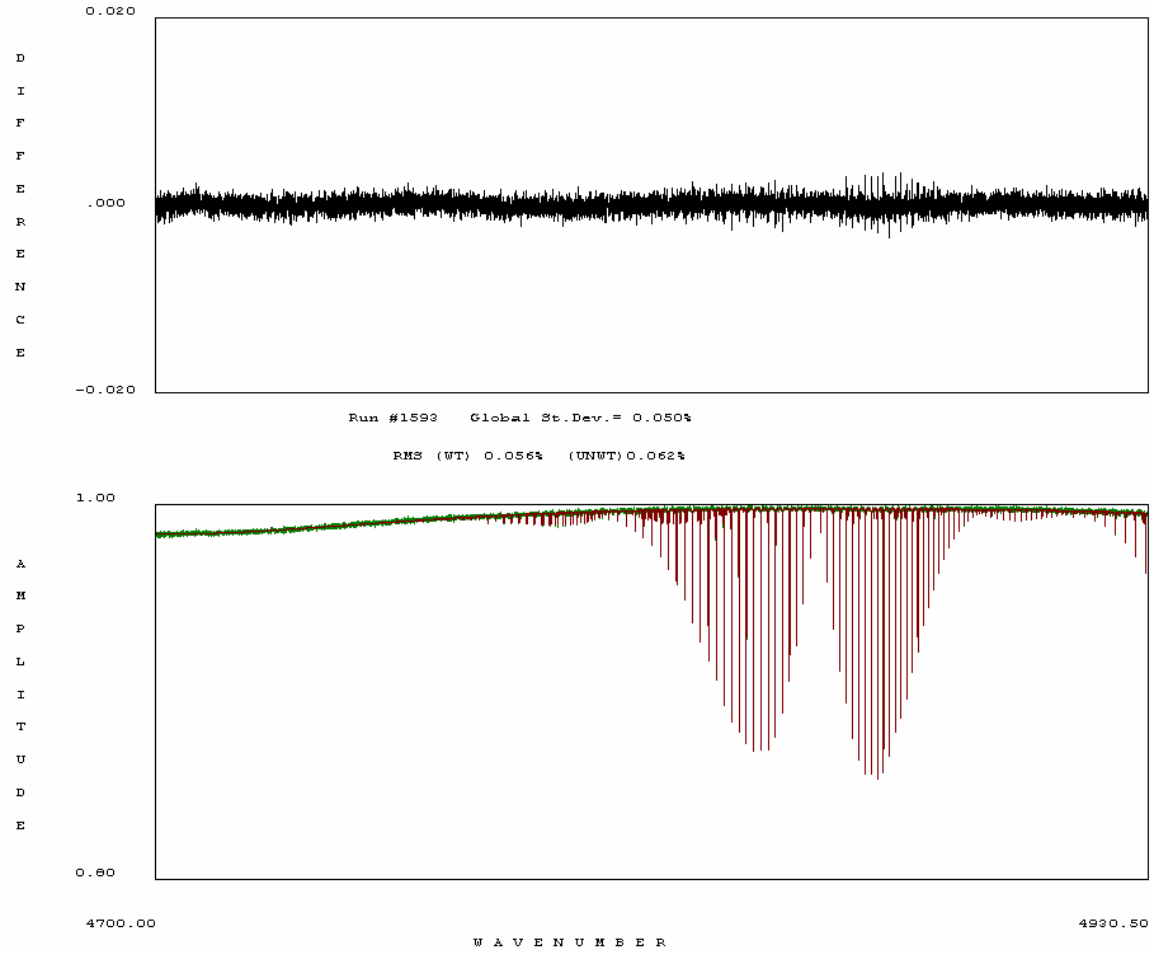

Fig. 9. Lower panel: spectrum 5 (green) and its fit (red), with amplitude on the y-axis and wavenumber in cm^{-1} on the x-axis. Upper panel: residuals of the fit.

Figure 9 depicts spectrum 5. The sample was .101 meters of CO_2, at 93.2 Torr and 22.60 degrees C. Its current weighting in the solution is 0.812.

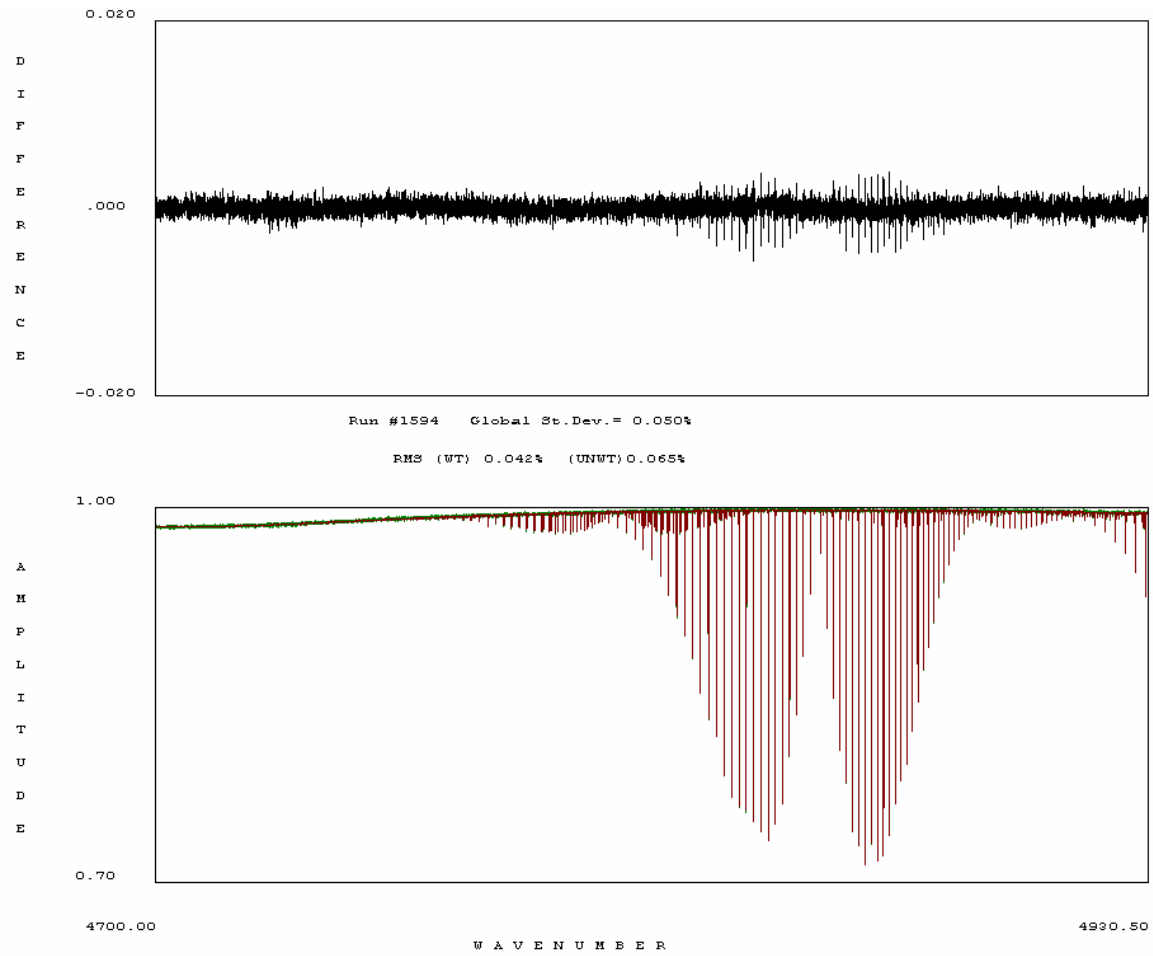

Fig. 10. Lower panel: spectrum 6 (green) and its fit (red), with amplitude on the y-axis and wavenumber in cm^{-1} on the x-axis. Upper panel: residuals of the fit.

Figure 10 depicts spectrum 6. The sample was 1.50 meters of CO_2, at 8.0 Torr and 22.40 degrees C. Its current weighting in the solution is 0.850.

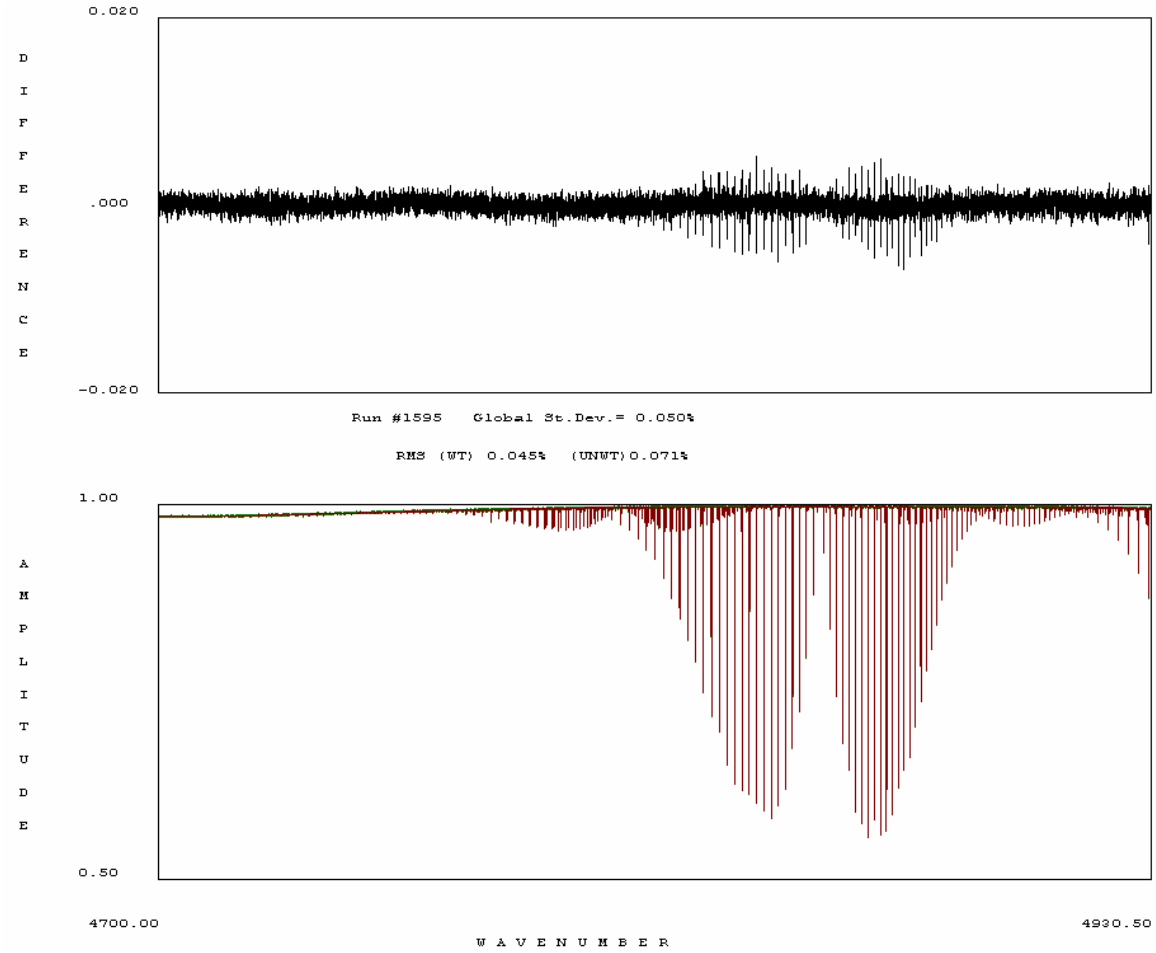

Fig. 11. Lower panel: spectrum 7 (green) and its fit (red), with amplitude on the y-axis and wavenumber in cm^{-1} on the x-axis. Upper panel: residuals of the fit.

Figure 11 depicts spectrum 7. The sample was 1.50 meters of CO_2, at 16.0 Torr and 22.30 degrees C. Its current weighting in the solution is 0.716. The dominant residuals in spectra 2 through 7 are due to unfitted effects such as line mixing or speed dependence. The errors on the positions, intensities, widths and shifts are extremely small for the 20013 ← 00001 band centered at 4854 cm^{-1} which is causing the residuals; therefore, systematic errors such as failure to account for line mixing or physical conditions during the data collection process are probably at fault.

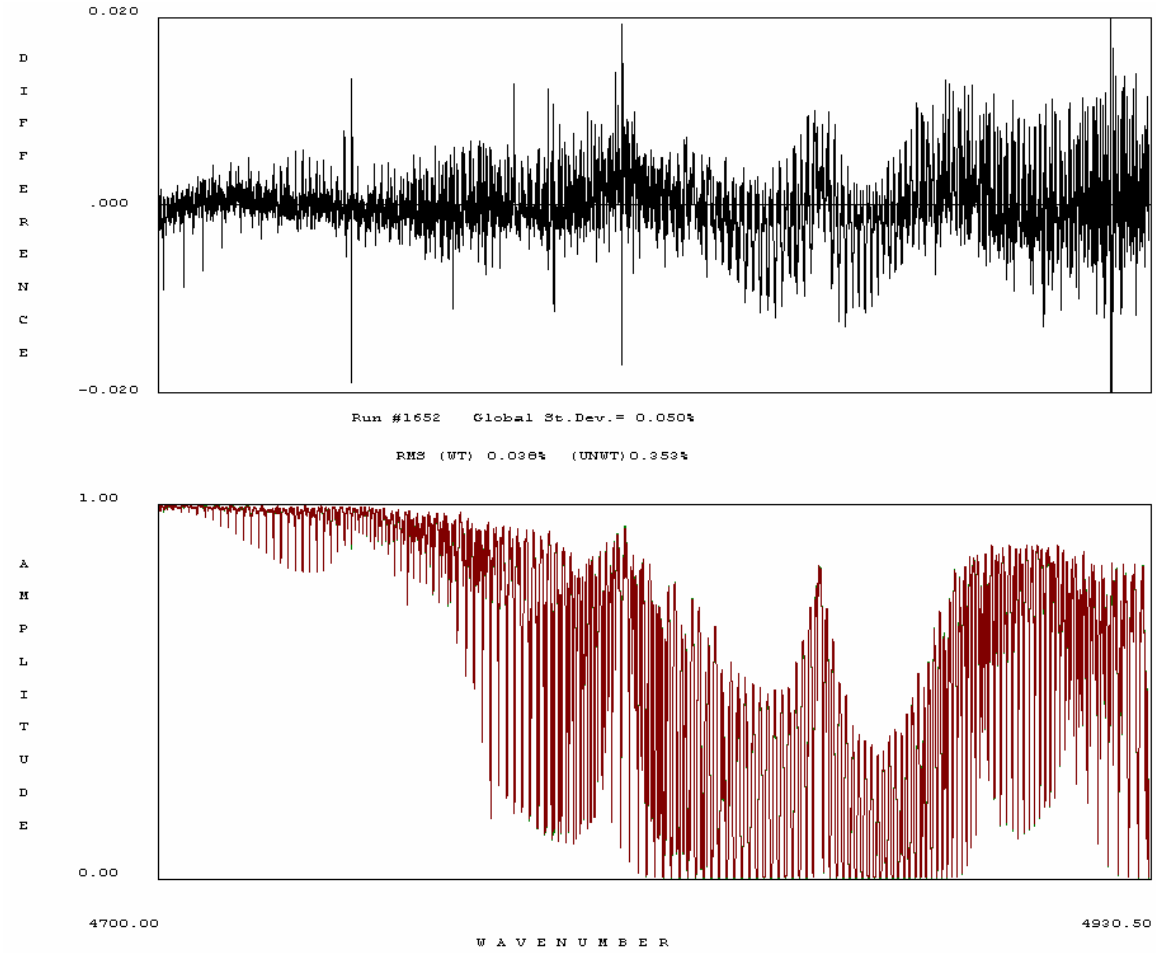

Fig. 12. Lower panel: spectrum 8 (green) and its fit (red), with amplitude on the y-axis and wavenumber in cm^{-1} on the x-axis. Note the extensive saturation of the spectrum in the 20013 ← 00001 band. Upper panel: residuals of the fit.

Figure 12 depicts spectrum 8. Spectra 8 through 11 were taken by Dr. Benner, Dr. Devi, Dr. Chip Miller, Emily Nugent, and me in January 2005 at the Kitt Peak FTS. Spectra 8 through 11 were recorded with a maximum path difference of 38.451 cm, and they are all unapodized. Note the overall strength of the spectral lines, especially the general saturation in the 20013 ← 00001 band. This spectrum serves much the same purpose as spectrum 714 in terms of identifying weak bands and lines, but it lacks the water contamination and high noise level of 714. Furthermore, since the strength of the spectral lines is due primarily to high pressure, rather than long path length, this spectrum is likely to exhibit pressure shift and width effects. The sample was 24.86 meters of CO_2, at 450.93 Torr and 20.74 degrees C. Because of its extremely complicated nature, its residuals could not be reduced to a level consistent with the other spectra in the solution: therefore, its current weighting is .0289.

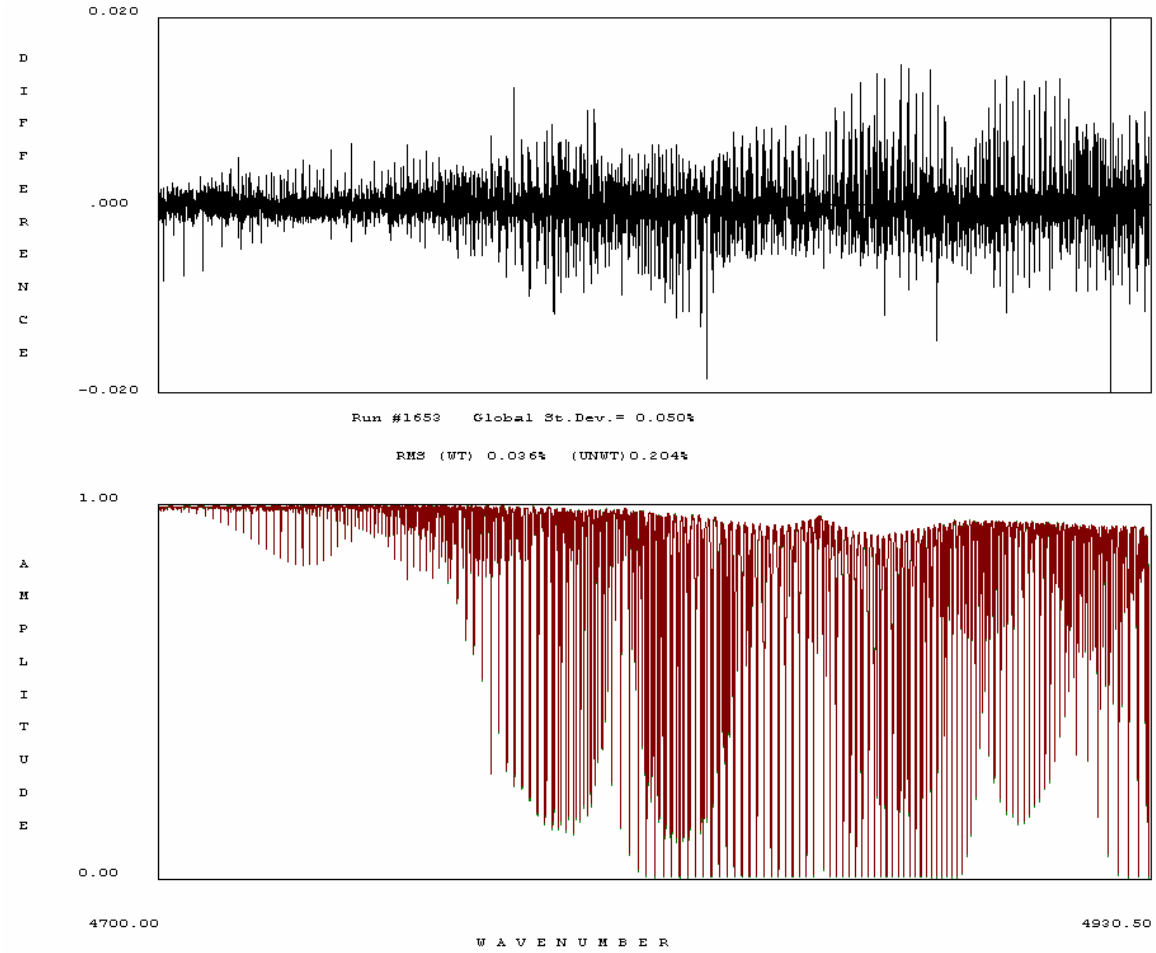

Fig. 13. Lower panel: spectrum 9 (green) and its fit (red), with amplitude on the y-axis and wavenumber on the x-axis. Upper panel: residuals of the fit.

Figure 13 depicts spectrum 9. The sample was 24.86 meters of CO_2, at 101.95 Torr and 20.73 degrees C. This spectrum has a relatively high pressure, but is not as intense as spectrum 8. Its current weighting in the solution is .0867.

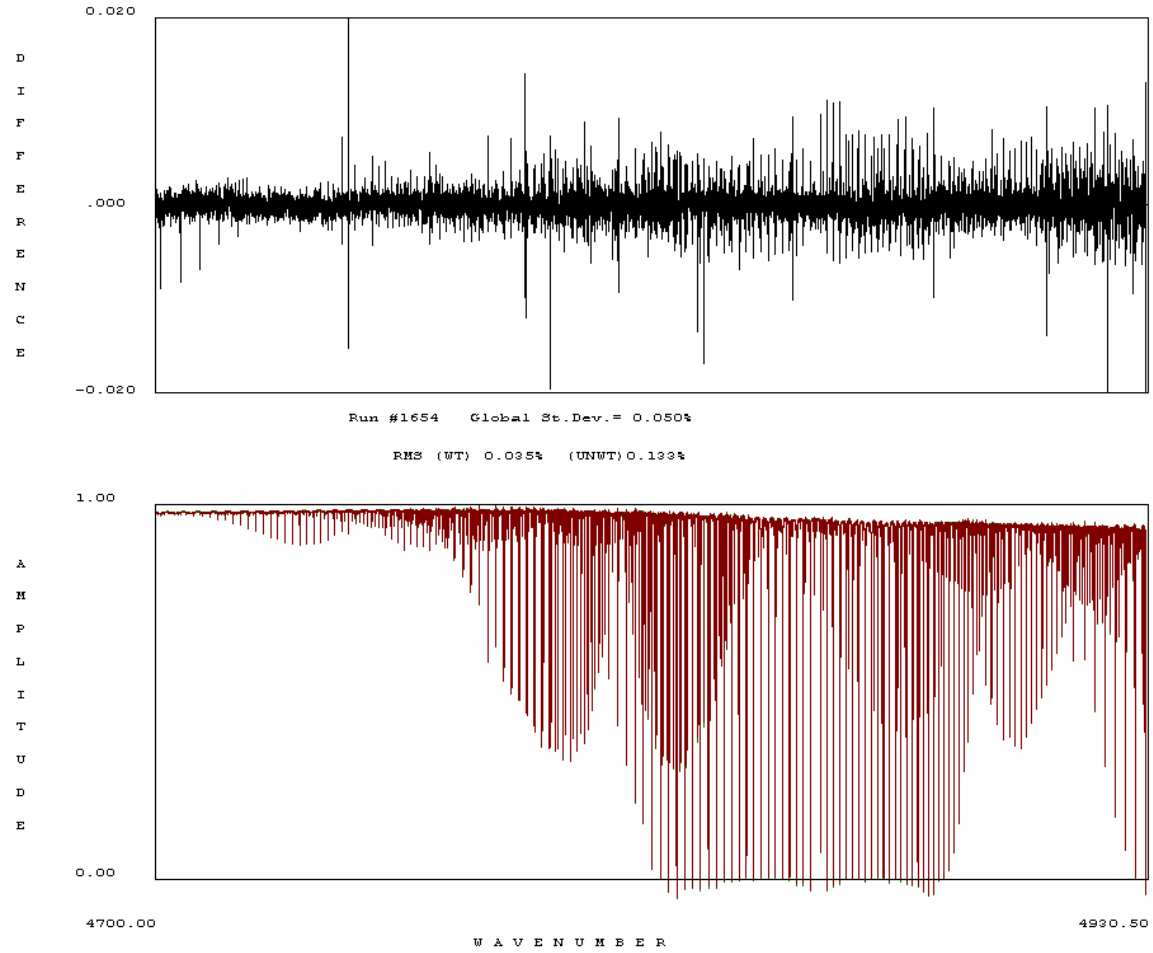

Fig. 14. Lower panel: spectrum 10 (green) and its fit (red), with amplitude on the y-axis and wavenumber on the x-axis. Upper panel: residuals of the fit.

Figure 14 depicts spectrum 10. Some of its spectral lines protrude below zero amplitude and above the source continuum due to the instrumental line shape, which introduces "ringing" around strong lines. The sample was 24.86 meters of CO_2, at 26.10 Torr and 20.79 degrees C. Its current weighting in the solution is 0.202.

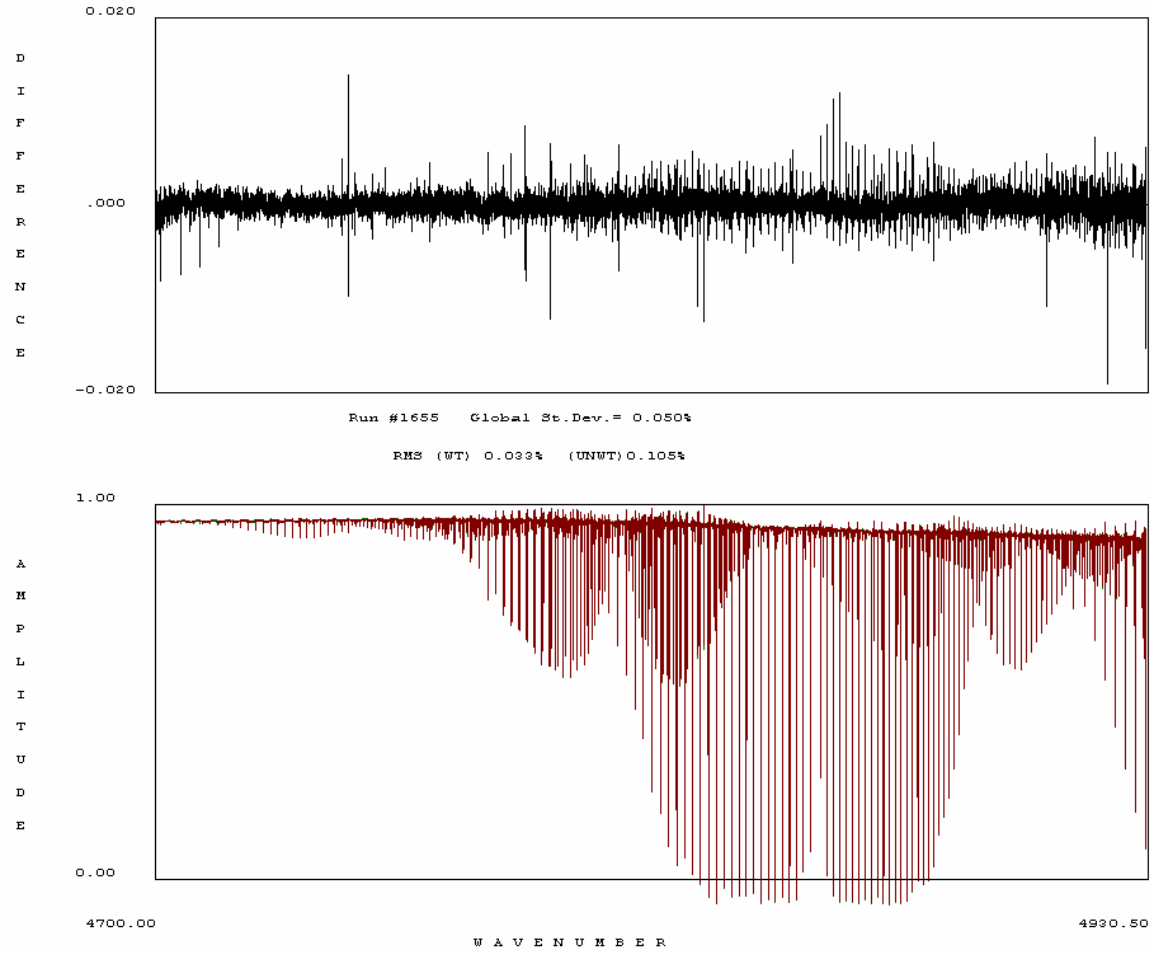

Fig. 15. Lower panel: spectrum 11 (green) and its fit (red), with amplitude on the y-axis and wavenumber on the x-axis. Upper panel: residuals of the fit.

Figure 15 depicts spectrum 11. The sample was 24.86 meters of CO_2, at 11.04 Torr and 20.90 degrees C. Its current weighting in the solution is 0.328.

Each spectrum from 2 through 7 has had its pressure in the solution modified to reduce the residuals of the fit. Because these spectra were received second-hand and the original experimenter expressed doubt regarding the accuracy of the pressures as given in the file headers, there was reason to believe that the pressures should be modified. Currently their pressures within the solution are 27 Torr, 64.4 Torr, 46.375 Torr, 87.4 Torr, 7.465 Torr, and 15.5 Torr respectively. The pressures of spectrum 1 and spectra 8 through 11 have not been modified. These values are summarized in Table 1.

Table 1: Pressures of the eleven spectra.

Spectrum	Original Pressure (Torr)	Modified Pressure (Torr)	Weight
1	79.00	79.00	0.044400
2	29.93	27.00	1.000000
3	70.20	64.40	0.832900
4	49.90	46.38	0.865900
5	93.20	87.40	0.811700
6	8.00	7.47	0.419300
7	16.00	15.50	0.400000
8	450.93	450.93	0.028898
9	101.95	101.95	0.086664
10	26.10	26.10	0.202051
11	11.04	11.04	0.327989

Each spectrum from 8 through 11 was found to contain a channel spectrum – a sine wave running through the spectrum likely caused by an etalonning in one of the spectrometer's optical components. An example of that channel spectrum is presented in Figure 16.

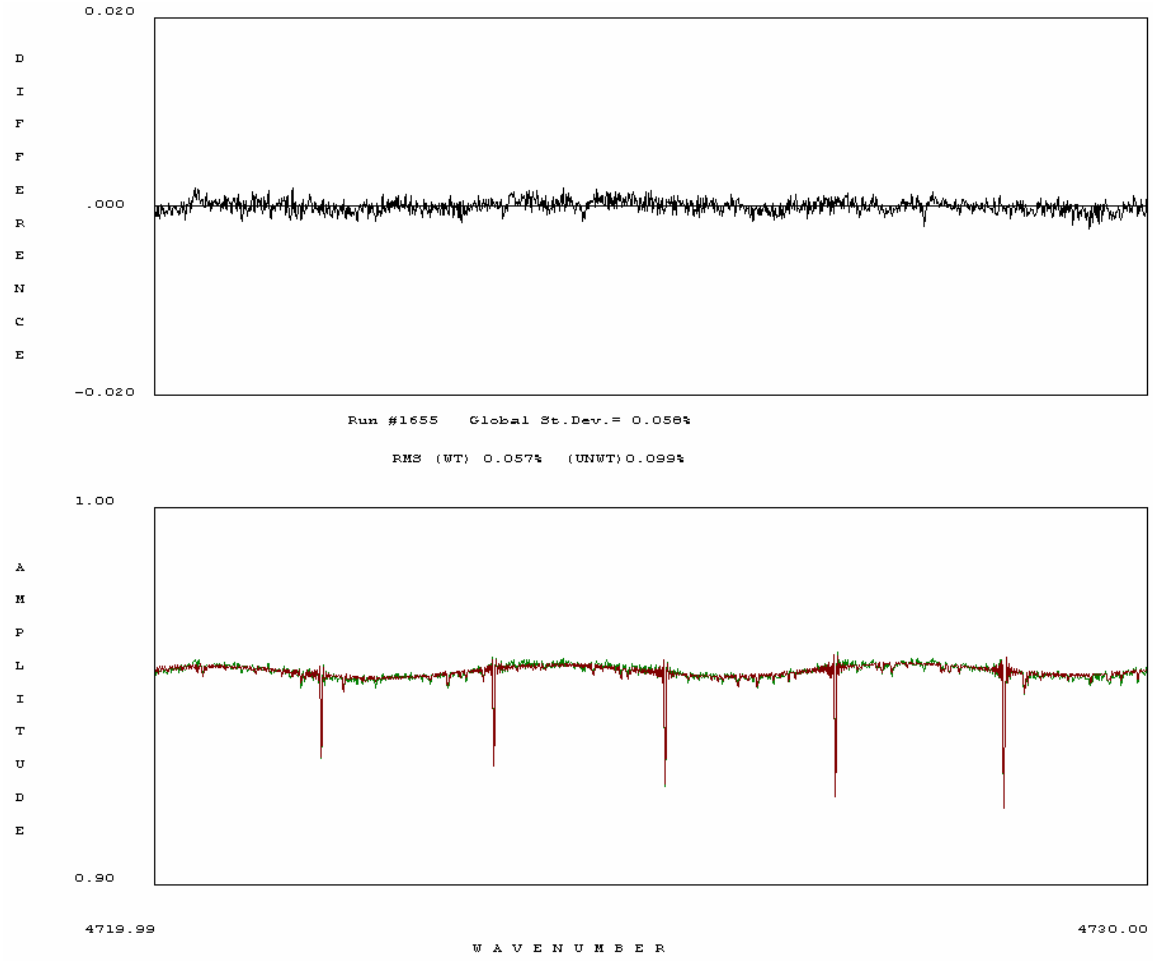

Fig. 16. Lower panel: a portion of spectrum 11 (green) and its fit (red), with amplitude on the y-axis and wavenumber on the x-axis. Note the sinusoidal wave running through the spectrum independent of the presence of spectral lines. This wave was fitted with a sine function with parameters as noted in Table 2. Upper panel: residuals of the fit.

A sinusoidal function was therefore added to the solution for each spectrum from that series in order to fit the effect. The parameters for that wave for each of those spectra, along with their related uncertainties, are presented in Table 2. All uncertainties presented in this paper represent one standard deviation of the relevant quantity.

Table 2: Channel spectrum parameters and uncertainties for spectra 8 through 11.

Spectrum	Amplitude (cm/atmosphere)	Period (1/cm)	Phase (1/cm)
8	0.002012	[1]	4804.505
Uncertainty	0.000043	[1]	0.013
9	0.001841	[1]	4804.505
Uncertainty	0.000017	[1]	0.005
10	0.001819	[1]	4804.519
Uncertainty	0.000010	[1]	0.003
11	0.001715	3.4987	4804.500
Uncertainty	0.000008	0.0001	[2]

[1] These parameters have been constrained to the period of the channel spectrum in spectrum 11 and thus have the same values and uncertainties.
[2] This parameter has been constrained to a constant and has no formal uncertainty.

The channel spectrum for spectrum 11 was determined first by measuring by eye the position of one of the peaks of the wave (to yield the phase) and dividing the total number of peaks over the spectrum by the spectrum's length (to yield the period). The values for the period and the amplitude were then unconstrained and iterated five times. Once the solution had stabilized the periods of the other three channel spectra were constrained to that of the first one, as the three periods should be the same assuming that a single mechanism was responsible for all three channel spectra. Their amplitudes and phases were initially set to those of the first channel spectrum, and were then unconstrained and allowed to iterate. This technique eliminated the large residuals resulting from the channel spectra.

The global standard deviation of the fit is 0.058%. The square root of the mean of the squares of the errors of each spectrum (Root Mean Square, or RMS) is presented in Table 3.

Table 3: Weighted and unweighted RMS by spectrum.

Spectrum	Weighted RMS (cm/molecule)	Unweighted RMS (cm/molecule)
1	0.05607	0.26582
2	0.06188	0.06188
3	0.05767	0.06319
4	0.05855	0.06292
5	0.05608	0.06224
6	0.06023	0.06534
7	0.06045	0.07142
8	0.05397	0.31751
9	0.05389	0.18307
10	0.05502	0.12240
11	0.05691	0.09937

5 Presentation of Results

The data tables are presented in an appendix to the report for convenience. Every intensity, self-induced pressure shift coefficient, and self-induced pressure broadening coefficient presented has been corrected to 296 Kelvins.

Tables 4 through 13 present the positions, intensities, and associated uncertainties for lines in ten vibrational bands for which those parameters have been unconstrained, organized by band and rotational state. The bands presented are the 31102 ← 00001, 12212 ← 00001, 20012 ← 00001, 21112 ← 01101, 30014 ← 10002, 30013 ← 10002, 22213 ← 02201, 30013 ← 10001, 00031 ← 11102, and 31113 ← 11102 bands of the $^{12}C^{16}O_2$ molecule.

The positions of lines in band 40002 ← 01101 and its interacting band of the $^{12}C^{16}O_2$ molecule have been constrained to functions according to the scheme presented in Equations 16 and 19, as have those in band 20013 ← 00001 of molecule $^{13}C^{16}O_2$. For the sake of conciseness only the underlying band constants which were unconstrained for those bands are presented in Tables 14 and 16, along with their associated uncertainties. Values for all other band constants occurring in Equations 16 and 19 are identical to those found in either Reference 11 or the HITRAN line list [9]. Uncertainties for individual line positions can be calculated according to Equation 20. The line intensities for those two bands are presented in Tables 15 and 17, respectively, along with their associated uncertainties.

The positions and intensities of lines in bands 20013 ← 00001 and 21113 ← 01101 of $^{12}C^{16}O_2$ and band 20012 ← 00001 of molecule $^{13}C^{16}O_2$ have been constrained to the functions presented in Equations 16, 17, and 18. The underlying band constants which were unconstrained for those bands are presented in Tables 18 through 20, along with their associated uncertainties. Values for all other band constants occurring in Equations 16 through 19 are identical to those found in either Reference 11 or the HITRAN line list [9]. Uncertainties for individual line parameters can be calculated according to Equation 20.

Tables 21 through 28 present the self-induced pressure broadening coefficients and self-induced pressure shift coefficients for lines in eight vibrational bands for which those parameters have been determined, organized by band and rotational state. The bands presented are the 20013 ← 00001, 20012 ← 00001, 21113 ← 01101, 40002 ← 01101, 21112 ← 01101, and 22213 ← 02201 bands of the $^{12}C^{16}O_2$ molecule, and the 20013 ← 00001 and 20012 ← 00001 bands of the $^{13}C^{16}O_2$ molecule. These tables list the positions of all lines they contain, regardless of whether they have been constrained to a function, in order to facilitate identification of any particular line. The unconstraining of these parameters was only possible through the use of constraint equations to constrain the positions of the lines. When the constraint equations are removed from the solution, it iterates to divergence immediately.

Of those eight bands, five exhibit lines roughly evenly distributed about the bandcenter. They are bands 20013 ← 00001, 21113← 01101, and 40002 ← 01101 of the $^{12}C^{16}O_2$ molecule, and bands 20013 ← 00001 and 20012 ← 00001 of the $^{13}C^{16}O_2$ molecule. Of those five, three exhibit generally small errors and localized distributions: bands 20013← 00001 and 21113 ← 01101 of the $^{12}C^{16}O_2$ molecule, and band

20012 ← 00001 of the $^{13}C^{16}O_2$ molecule. Those three bands of note are Tables 21, 23, and 28, respectively.

The errors presented in the above tables are representative of the random errors due to noise in the fitted spectra and correlations between the floated parameters only. They do not include systematic errors such as uncertainties in data collection or improper modeling of the spectrum.

Figure 17 presents a comparison of self-broadening coefficients between this work and the 2000 HITRAN line list for bands 20013 ← 00001 and 21113← 01101 of the $^{12}C^{16}O_2$ molecule, and band 20012 ← 00001 of the $^{13}C^{16}O_2$ molecule. There is significant variation for nearly all of the values. No error bars are presented for the HITRAN data, as the database does not include errors with its measurements. No similar comparison is possible for pressure shift coefficients, as the HITRAN line list does not list them.

Figure 18 presents the self-broadening coefficients of each line in all eight bands for which they are determined as a function of the absolute value of the quantum number m. Implicit in the 2000 HITRAN CO_2 line list is the assumption that any two lines, regardless of branch or band, which share the same absolute value of m have the same self-broadening coefficient. The HITRAN lists the same self-broadening coefficient for every set of lines with the same value of |m|. However, Figure 18 displays marked variation from band to band. The error bars have been removed from this figure for clarity.

Figure 19 is an enlargement of the left-central portion of Figure 18, with the error bars restored and the least well-determined bands removed for clarity. It presents bands 20013 ← 00001 and 21113← 01101 of the $^{12}C^{16}O_2$ molecule, and band 20012 ← 00001 of the $^{13}C^{16}O_2$ molecule. For a given value of |m|, the self-broadening coefficients vary significantly from band to band and even from line to line.

Figure 20 presents the self-shift coefficients of each line in all eight bands for which they are determined as a function of wavenumber in cm^{-1}. Note the predominantly negative values for the self-shift coefficient. The error bars have been removed from this figure for clarity.

Figure 21 is a section of Figure 20, presenting only bands 20013 ← 00001 and 21113← 01101 of the $^{12}C^{16}O_2$ molecule, and band 20012 ← 00001 of the $^{13}C^{16}O_2$ molecule, and their associated error bars. The self-shift coefficients for these bands remain at all times below zero, and their uncertainties are in general small.

Figure 22 is a section of Figure 20, presenting only bands 40012 ← 01101 and 22213← 02201 of the $^{12}C^{16}O_2$ molecule, and band 20013 ← 00001 of the $^{13}C^{16}O_2$ molecule, and their associated error bars. The self-shift coefficients for these bands often range above zero; however, their uncertainties are large. The uncertainties are smallest for those lines whose distribution in the wavenumber-self-shift plane approaches that of bands 20013 ← 00001 and 21113 ← 01101 of the $^{12}C^{16}O_2$ molecule, or band 20012 ← 00001 of the $^{13}C^{16}O_2$ molecule; for those lines which fall above the x-axis, the uncertainties are very large.

Figure 23 presents the self-shift coefficients of each line in all eight bands for which they are determined as a function of quantum number m. The close resemblance in profile from band to band is clearer when the data are lined up with their peaks at m = 0. The error bars have been removed from this figure for clarity.

Figure 24 is a section of Figure 23, presenting only bands 20013 ← 00001 and 21113← 01101 of the $^{12}C^{16}O_2$ molecule, and band 20012 ← 00001 of the $^{13}C^{16}O_2$ molecule, and their associated error bars. The bands' profiles are nearly the same near m = 0, and as they diverge towards the edges their uncertainties increase.

Figure 25 is a section of Figure 23, presenting only bands 40012 ← 01101 and 22213← 02201 of the $^{12}C^{16}O_2$ molecule, and band 20013 ← 00001 of the $^{13}C^{16}O_2$ molecule, and their associated error bars. Despite the large uncertainties on these data points, they still exhibit a rising profile towards the center.

6 Conclusions

The α_l self-induced pressure-broadening coefficient and the δ self-induced pressure-shift coefficient have been determined for approximately 470 spectral lines, with a degree of precision as great as 7.00E-05 cm^{-1}/atm for α_l, and 1.20E-04 cm^{-1}/atmosphere for δ. A weak correlation has been demonstrated between the pressure broadening coefficients of spectral lines with identical absolute values of the quantum number m. This correlation does not extend to the lines' pressure-broadening coefficient being the same across bands, or even across the P and R branches within a single band. Percent errors for α_l and δ were found to average 1.3% and 16.4% respectively. This experiment has failed to attain the precision of greater than 0.3% desired for characterization of CO_2 sinks and sources on a regional scale; nevertheless, it does represent a significant improvement over the HITRAN spectroscopic database's values for α_l and δ. The technique of multispectrum least-squares fitting has been shown to be effective for attaining high precision in measurement of spectral parameters even given nonideal data. Additional fitting on the spectra currently in the solution, especially the constraint of more spectral line parameters to functions, may improve the fit, and thus the precision with which spectral parameters can be determined. Furthermore, the addition of spectra taken at a wide range of temperatures may allow this solution to encompass the temperature-dependence exponent n.

7 References

[1] D. C. Benner, C. P. Rinsland, V. M. Devi, M. A. H. Smith and D. Atkins, "A Multispectrum Nonlinear Least Squares Fitting Technique," J. Quant. Spectrosc. Radiat. Transfer **53**, 705 (1995).

[2] "KILIMANJARO-MAP." Mountain Watch Media Launch, October 23rd 2002. Available May 05, 2005 at http://www.unep-wcmc.org/information_services/publications/MountainWatch_Bishkek/presspack/I/KILIMANJARO-MAP.JPG

[3] R. T. Watson, C. W. Team "Climate Change 2001: Synthesis Report," Intergovernmental Panel on Climate Change, 2001.

[4] L. Wallace, W. Livingstone, J. Geophys. Res. D 95 (1990) 9823-9827.

[5] D. Crisp. "The Orbiting Carbon Observatory," COSPAR, 2003, Houston TX.

[6] D. M. O'Brien, P. J. Rayner, J. Geophys. Res. D 107 (2002) 4354.

[7] P. J. Rayner, R. M. Law, D. M. O'Brien, T. M. Butler, A. C. Dilley, J. Geophys. Res. D 107 (2002) 4557.

[8] Z. H. Yang, G. C. Toon, J. S. Margolis, P. O. Wennberg, Geophys. Res. Lett. 29 (2002) 1339.

[9] L.S. Rothman, A. Barbe, D.C. Benner, L.R. Brown, C. Camy-Peyret, M.R. Carleer, K. Chance, C. Clerbaux, V. Dana, V.M. Devi, A. Fayt, J.-M. Flaud, R.R. Gamache, A. Goldman, D. Jacquemart, K.W. Jucks, W.J. Lafferty, J.-Y. Mandin, S.T. Massie, V. Nemtchinov, D.A. Newnham, A. Perrin, C.P. Rinsland, J. Schroeder, K.M. Smith, M.A.H. Smith, K. Tang, R.A. Toth, J. Vander Auwera, P. Varanasi and K. Yoshino, "The HITRAN molecular spectroscopic database: edition of 2000 including updates through 2001," J. Quant. Spectrosc. Radiat. Transfer 82 (2003) 5-44.

[10] V. Dana, J.-Y. Mandin, C. Camy-Peyret, J.-M. Flaud, J.-P. Chevillard, R. L. Hawkins, and J.-L. Delfau, Appl. Opt. **31**, 1928 (1992).

[11] Charles E. Miller and Linda R. Brown, "Near Infrared Spectroscopy of Carbon Dioxide I. $^{16}O^{12}C^{16}O$ Line Positions," J. Mol. Spectrosc. 228 (2004) 329-354.

[12] D. Mihalas, Stellar Atmospheres. Chicago: W. H. Freeman and Co., 1970.

[13] Sumner P. Davis, Mark C. Abrams and James W. Brault, Fourier Transform Spectroscopy. San Diego: Academic Press, 2001.

[14] V. Malathy Devi, D. Chris Benner, C. P. Rinsland, M. A. H. Smith, and D. S. Parmar. "Infrared Spectroscopy of the CO_2 molecule." Recent Res. Devel. In Geophys. Res., 1 (1996) 119-148.

[15] Mike Dulick, Claude Plymate, Jeremy Wagner. "One-Meter Fourier Transform Spectrometer." Available May 05, 2005 at http://www.noao.edu/noao/staff/plymate/fts/aboutFTS.html

[16] J. U. White, J. Opt. Soc. Am. 32, 285 (1942).

Table 4: Line Positions and Intensities
for band 31102 ← 00001 of molecule 12C 16O2
Values corrected to 296K

	J"	Line Position (1/cm)	Position (1/cm)	Line Intensity (cm/molecule)	Intensity (cm/molecule)
P	40	4721.505581	0.001666	2.80E-26	3.3E-27
P	36	4724.763089	0.000932	5.56E-26	3.5E-27
P	34	4726.384373	0.001181	4.10E-26	2.7E-27
P	32	4728.003860	0.001180	4.15E-26	3.0E-27
P	30	4729.622100	Fixed	4.09E-26	2.8E-27
P	28	4731.238582	0.000859	6.02E-26	2.8E-27
P	26	4732.845125	0.001243	4.40E-26	3.3E-27
R	12	4763.504967	0.000706	8.39E-26	3.7E-27
R	14	4765.035353	0.000554	1.020E-25	3.1E-27
R	16	4766.562808	0.000483	1.161E-25	3.4E-27
R	18	4768.085458	0.000468	1.224E-25	3.9E-27
R	20	4769.604530	0.000369	1.503E-25	3.3E-27
R	22	4771.119892	0.000378	1.440E-25	3.0E-27
R	24	4772.630337	0.000357	1.653E-25	4.1E-27
R	26	4774.137181	0.000350	1.519E-25	2.9E-27
R	28	4775.640404	0.000379	1.412E-25	3.7E-27
R	32	4778.633900	0.000402	1.257E-25	3.0E-27
R	36	4781.611081	0.000476	1.034E-25	2.8E-27
R	38	4783.095077	0.000511	9.52E-26	2.9E-27

Table 5: Line Positions and Intensities
for band 12212 ← 00001 of molecule 12C 16O2
Values corrected to 296K

	J''	Line Position (1/cm)	Position Uncertainty (1/cm)	Line Intensity (cm/molecule)	Intensity Uncertainty (cm/molecule)
P	50	4845.908866	0.001160	5.18E-26	4.8E-27
P	48	4847.710534	0.000827	5.99E-26	3.4E-27
P	46	4849.501989	0.000588	8.36E-26	3.2E-27
P	44	4851.282891	0.000524	9.67E-26	3.3E-27
P	42	4853.054899	0.000515	9.83E-26	3.1E-27
P	40	4854.816380	0.000442	1.190E-25	3.4E-27
P	38	4856.567070	0.000353	1.493E-25	3.3E-27
P	36	4858.309677	0.000407	1.328E-25	3.5E-27
P	34	4860.041063	0.000485	1.160E-25	3.8E-27
P	32	4861.763353	0.000706	9.03E-26	4.9E-27
P	26	4866.871482	0.000616	9.85E-26	4.1E-27
P	24	4868.554713	0.000793	7.76E-26	4.1E-27
P	22	4870.224100	Fixed	5.60E-26	5.2E-27
P	18	4873.545179	0.002160	2.80E-26	3.9E-27
P	12	4878.450410	0.001136	5.82E-26	4.4E-27
R	26	4908.080309	0.000539	1.099E-25	3.7E-27
R	34	4913.672770	0.000329	1.706E-25	3.3E-27
R	44	4920.422069	0.000638	1.118E-25	4.9E-27

Table 6: Line Positions and Intensities
for band 20012 ← 00001 of molecule 12C 16O2
Values corrected to 296K

	J"	Line Position (1/cm)	Position Uncertainty (1/cm)	Line Intensity (cm/molecule)	Intensity Uncertainty (cm/molecule)
P	80	4892.504763	0.001170	3.70E-26	2.8E-27
P	78	4895.172106	0.000604	7.18E-26	2.7E-27
P	76	4897.820376	0.000376	1.406E-25	3.9E-27
P	74	4900.443726	0.000289	2.355E-25	6.4E-27
P	72	4903.041727	0.000111	4.211E-25	2.9E-27
P	70	4905.614505	0.000071	6.899E-25	3.2E-27
P	68	4908.161786	0.000077	1.188E-24	6 E-27
P	66	4910.681013	0.000041	1.943E-24	1 E-26
P	62	4915.639423	0.000021	4.810E-24	7 E-27
P	60	4918.077149	0.000016	7.349E-24	9 E-27
P	58	4920.487101	0.000013	1.130E-23	1 E-26
P	56	4922.868984	0.000011	1.693E-23	2 E-26
P	54	4925.222555	0.000010	2.465E-23	4 E-26
P	52	4927.547832	0.000009	3.560E-23	6 E-26
P	50	4929.844660	0.000009	5.073E-23	1.0E-25

Table 7: Line Positions and Intensities
for band 21112 ← 01101 of molecule 12C 16O2
Values corrected to 296K

	J"	Line Position (1/cm)	Position Uncertainty (1/cm)	Line Intensity (cm/molecule)	Intensity Uncertainty (cm/molecule)
P	71	4892.153200	Fixed	1.39E-26	2.7E-27
P	70	4895.665462	0.002240	1.94E-26	3.2E-27
P	68	4898.074740	0.001813	2.42E-26	3.0E-27
P	67	4897.229405	0.000778	6.09E-26	3.6E-27
P	62	4905.149918	0.000281	1.654E-25	2.8E-27
P	60	4907.459573	0.000188	2.556E-25	3.0E-27
P	57	4909.413619	0.000164	4.648E-25	4.6E-27
P	56	4912.007889	0.000129	5.677E-25	4.4E-27
P	55	4911.767123	0.000119	6.814E-25	5.8E-27
P	54	4914.245673	0.000090	8.335E-25	4.6E-27
P	53	4914.092285	0.000076	9.838E-25	3.7E-27
P	52	4916.456395	0.000070	1.225E-24	5 E-27
P	51	4916.389801	0.000061	1.495E-24	7 E-27
P	49	4918.657601	0.000048	2.330E-24	6 E-27
P	48	4920.812711	0.000038	2.440E-24	6 E-27
P	47	4920.899328	0.000033	2.860E-24	6 E-27
P	46	4922.952851	0.000034	3.335E-24	7 E-27
P	45	4923.112279	0.000027	3.895E-24	7 E-27
P	44	4925.068850	0.000025	4.507E-24	8 E-27
P	43	4925.297002	0.000024	5.248E-24	9 E-27
P	42	4927.160849	0.000023	5.136E-24	8 E-27
P	41	4927.453554	0.000020	6.883E-24	1.1E-26
P	40	4929.227361	0.000017	7.838E-24	1 E-26
P	39	4929.581916	0.000016	8.875E-24	1.1E-26

Table 8: Line Positions and Intensities
for band 30014 ← 10002 of molecule 12C 16O2
Values corrected to 296K

	J"	Line Position (1/cm)	Position Uncertainty (1/cm)	Line Intensity (cm/molecule)	Intensity Uncertainty (cm/molecule)
P	52	4745.503006	Fixed	3.58E-26	2.9E-27
P	50	4747.424611	0.000819	5.79E-26	2.7E-27
P	48	4749.327491	0.000562	8.48E-26	3.1E-27
P	46	4751.217719	0.000461	1.048E-25	3.2E-27
P	44	4753.089142	0.000344	1.405E-25	2.8E-27
P	40	4756.783126	0.000211	2.441E-25	2.9E-27
P	38	4758.606131	0.000169	3.099E-25	2.9E-27
P	36	4760.413758	0.000138	3.895E-25	3.2E-27
P	34	4762.206039	0.000117	4.778E-25	3.8E-27
P	32	4763.983482	0.000097	5.803E-25	3.5E-27
P	30	4765.746415	0.000084	6.741E-25	3.3E-27
P	28	4767.494888	0.000074	7.875E-25	3.5E-27
P	26	4769.229196	0.000067	8.897E-25	3.6E-27
P	24	4770.949728	0.000062	9.945E-25	3.7E-27
P	22	4772.656584	0.000062	1.087E-24	5 E-27
P	20	4774.349931	0.000055	1.156E-24	4 E-27
P	18	4776.029874	0.000053	1.221E-24	4 E-27
P	16	4777.696817	0.000053	1.249E-24	4 E-27
P	14	4779.350556	0.000055	1.215E-24	4 E-27
P	8	4784.235346	0.000075	9.109E-25	3.9E-27
P	6	4785.838283	0.000095	7.149E-25	3.7E-27
P	4	4787.428574	0.000135	5.053E-25	3.8E-27
P	2	4789.006068	0.000283	2.573E-25	4.6E-27
R	2	4792.894997	0.000179	3.873E-25	3.9E-27
R	4	4794.428615	0.000107	6.331E-25	3.8E-27
R	6	4795.948957	0.000081	8.505E-25	3.8E-27
R	8	4797.457064	0.000067	1.024E-24	4 E-27
R	10	4798.951952	0.000059	1.174E-24	4 E-27
R	14	4801.902053	0.000051	1.330E-24	4 E-27
R	16	4803.357059	0.000070	1.309E-24	6 E-27
R	18	4804.798135	0.000050	1.305E-24	4 E-27
R	20	4806.225728	0.000060	1.133E-24	5 E-27
R	22	4807.638077	0.000071	1.100E-24	9 E-27
R	24	4809.037592	0.000059	1.049E-24	4 E-27
R	26	4810.421867	0.000065	9.534E-25	4.0E-27
R	28	4811.791002	0.000070	8.390E-25	3.6E-27
R	30	4813.145095	0.000083	7.245E-25	4.2E-27
R	32	4814.483524	0.000095	6.193E-25	4.2E-27
R	34	4815.806040	0.000110	5.032E-25	3.4E-27
R	36	4817.112210	0.000143	4.029E-25	4.0E-27
R	38	4818.401928	0.000165	3.225E-25	3.2E-27
R	40	4819.674968	0.000220	2.424E-25	3.3E-27
R	46	4823.386916	0.000406	1.277E-25	3.8E-27
P	58	4884.736626	0.001855	2.39E-26	2.9E-27

Table 9: Line Positions and Intensities
for band 30013 ← 10002 of molecule 12C 16O2
Values corrected to 296K

	J"	Line Position (1/cm)	Position (1/cm)	Line Intensity (cm/molecule)	Intensity (cm/molecule)
P	54	4889.541260	0.000534	9.06E-26	3.0E-27
P	52	4891.896572	0.000390	1.263E-25	3.1E-27
P	50	4894.223224	0.000266	1.911E-25	3.3E-27
P	48	4896.518387	0.000206	2.547E-25	3.3E-27
P	44	4901.017184	0.000112	4.992E-25	3.9E-27
P	42	4903.220723	0.000084	6.697E-25	3.5E-27
P	40	4905.394255	0.000065	8.810E-25	3.4E-27
P	36	4909.649243	0.000045	1.390E-24	4 E-27
P	34	4911.731487	0.000039	1.740E-24	5 E-27
P	32	4913.783208	0.000034	2.102E-24	5 E-27
P	30	4915.804635	0.000029	2.491E-24	6 E-27
P	28	4917.795936	0.000025	2.934E-24	5 E-27
P	26	4919.756805	0.000023	3.419E-24	5 E-27
P	24	4921.687641	0.000023	3.698E-24	7 E-27
P	22	4923.588190	0.000020	4.090E-24	6 E-27
P	20	4925.458717	0.000020	4.366E-24	7 E-27
P	18	4927.299026	0.000019	4.558E-24	7 E-27
P	16	4929.109325	0.000019	4.655E-24	7 E-27

Table 10: Line Positions and Intensities
for band 22213 ← 02201 of molecule 12C 16O2
Values corrected to 296K

	J"	Line Position (1/cm)	Position Uncertainty (1/cm)	Line Intensity (cm/molecule)	Intensity Uncertainty (cm/molecule)
P	51	4722.756879	0.002834	1.64E-26	2.6E-27
P	49	4724.788100	Fixed	2.28E-26	3.4E-27
P	48	4725.975460	Fixed	2.98E-26	2.8E-27
P	47	4726.803184	0.001708	2.80E-26	3.2E-27
P	45	4728.792862	0.001087	4.40E-26	3.2E-27
P	43	4730.761663	0.000773	6.26E-26	2.7E-27
P	42	4731.843480	Fixed	6.84E-26	3.1E-27
P	41	4732.712274	0.000581	8.46E-26	2.8E-27
P	40	4733.763150	Fixed	8.56E-26	2.9E-27
P	39	4734.642720	0.000646	1.067E-25	4.2E-27
P	37	4736.553987	0.000504	1.442E-25	4.5E-27
P	35	4738.445213	0.000480	1.611E-25	4.9E-27
P	32	4741.280410	Fixed	2.231E-25	4.2E-27
P	31	4742.171058	0.000305	2.521E-25	4.1E-27
P	30	4743.117782	0.000290	2.721E-25	4.4E-27
P	29	4744.005300	0.000266	2.948E-25	4.2E-27
P	27	4745.821276	0.000234	3.351E-25	4.3E-27
P	26	4746.737542	0.000222	3.554E-25	4.5E-27
P	25	4747.618792	0.000213	3.773E-25	4.5E-27
P	24	4748.521676	0.000206	3.892E-25	4.4E-27
P	23	4749.397828	0.000199	4.065E-25	5.2E-27
P	22	4750.288231	0.000195	4.208E-25	4.8E-27
P	21	4751.158191	0.000181	4.505E-25	4.9E-27
P	20	4752.036895	0.000177	4.656E-25	4.9E-27
P	19	4752.900220	0.000163	5.036E-25	4.7E-27
P	18	4753.768808	0.000171	4.959E-25	4.7E-27
P	17	4754.624836	0.000169	4.968E-25	4.7E-27
P	16	4755.482045	0.000173	4.929E-25	5.0E-27
P	15	4756.330811	0.000178	4.850E-25	5.0E-27
P	14	4757.178153	0.000180	4.652E-25	4.7E-27
P	12	4758.856870	0.000192	4.466E-25	5.8E-27
P	11	4759.688557	0.000201	4.281E-25	4.8E-27
P	9	4761.339786	0.000235	3.738E-25	4.9E-27
P	8	4762.160412	0.000263	3.468E-25	5.6E-27
P	7	4762.974616	0.000297	3.102E-25	4.8E-27
P	4	4765.390986	0.000656	1.556E-25	6.0E-27
P	3	4766.188265	0.001121	6.06E-26	4.1E-27
Q	28	4766.715118	0.002401	2.11E-26	3.2E-27
Q	17	4767.818105	0.001907	4.22E-26	4.6E-27
Q	13	4768.145083	0.002262	2.52E-26	3.6E-27
Q	12	4768.199900	Fixed	2.50E-26	3.6E-27
Q	11	4768.257740	0.001620	3.63E-26	3.3E-27
R	2	4770.875613	0.000744	8.87E-26	3.9E-27
R	4	4772.400727	0.000448	2.133E-25	5.8E-27
R	6	4773.910054	0.000293	3.156E-25	6.7E-27
R	7	4774.656913	0.000249	3.605E-25	5.0E-27
R	10	4776.871748	0.000194	4.550E-25	4.8E-27
R	12	4778.325473	0.000173	4.827E-25	4.6E-27
R	14	4779.761445	0.000166	5.259E-25	5.3E-27
R	15	4780.469847	0.000170	5.268E-25	6.3E-27
R	16	4781.179214	0.000166	5.322E-25	5.2E-27
R	17	4781.876797	0.000159	5.283E-25	4.7E-27
R	19	4783.265427	0.000158	5.297E-25	4.6E-27
R	20	4783.960366	0.000163	5.089E-25	4.6E-27
R	21	4784.635188	0.000192	5.124E-25	6.0E-27
R	22	4785.323906	0.000178	4.714E-25	4.9E-27

Band 22213 ← 02201 of molecule 12C 16O2 continues
Values corrected to 296K

	J''	Line Position (1/cm)	Position Uncertainty (1/cm)	Line Intensity (cm/molecule)	Intensity Uncertainty (cm/molecule)
R	24	4786.669387	0.000199	4.418E-25	5.3E-27
R	25	4787.317511	0.000198	4.087E-25	4.6E-27
R	26	4787.996590	0.000234	3.909E-25	5.4E-27
R	27	4788.630052	0.000226	3.689E-25	4.8E-27
R	28	4789.305929	0.000234	3.383E-25	4.4E-27
R	29	4789.923028	0.000260	3.130E-25	4.8E-27
R	31	4791.196324	0.000304	2.605E-25	4.7E-27
R	33	4792.449501	0.000337	2.210E-25	4.2E-27
R	41	4797.260695	0.000578	8.59E-26	3.1E-27
R	43	4798.411683	0.000793	6.24E-26	3.1E-27

Table 11: Line Positions and Intensities
for band 30013 ← 10001 of molecule 12C 16O2
Values corrected to 296K

	J"	Line Position (1/cm)	Position Uncertainty (1/cm)	Line Intensity (cm/molecule)	Intensity Uncertainty (cm/molecule)
P	42	4800.838370	Fixed	6.88E-26	2.9E-27
P	38	4805.102978	0.000428	1.188E-25	3.0E-27
P	32	4811.270078	0.000248	2.354E-25	4.7E-27
P	30	4813.264977	0.000210	2.770E-25	3.9E-27
P	28	4815.230086	0.000187	3.458E-25	4.9E-27
P	26	4817.166097	0.000171	3.676E-25	4.5E-27
P	22	4820.950561	0.000156	4.259E-25	4.8E-27
P	20	4822.798673	0.000134	4.909E-25	4.6E-27
P	18	4824.618735	0.000138	5.217E-25	5.8E-27
P	16	4826.410053	0.000132	5.020E-25	4.4E-27
P	14	4828.173305	0.000133	5.027E-25	4.5E-27
P	12	4829.907972	0.000145	4.922E-25	5.2E-27
P	10	4831.615295	0.000155	4.354E-25	4.2E-27
P	8	4833.294301	0.000177	3.825E-25	4.1E-27
P	6	4834.946389	0.000361	3.046E-25	5.9E-27
P	4	4836.568753	0.000328	2.149E-25	4.1E-27
P	2	4838.164657	0.000512	1.356E-25	3.9E-27
R	2	4842.031634	0.000463	1.603E-25	4.8E-27
R	4	4843.529459	0.000259	2.751E-25	4.4E-27
R	6	4844.999763	0.000179	3.820E-25	4.1E-27
R	8	4846.441806	0.000149	4.523E-25	4.0E-27
R	10	4847.853782	0.000158	4.495E-25	4.3E-27
R	12	4849.241292	0.000130	5.146E-25	4.2E-27
R	14	4850.598359	0.000130	5.587E-25	5.4E-27
R	16	4851.926802	0.000115	5.894E-25	4.7E-27
R	18	4853.226336	0.000115	5.424E-25	3.5E-27
R	20	4854.496874	0.000119	5.541E-25	4.7E-27
R	22	4855.738200	0.000134	4.798E-25	4.4E-27
R	24	4856.949989	0.000135	4.514E-25	3.9E-27
R	26	4858.131766	0.000136	4.393E-25	3.8E-27
R	28	4859.283730	0.000161	3.766E-25	4.1E-27
R	32	4861.495497	0.000217	2.683E-25	3.9E-27
R	34	4862.555959	0.000225	2.534E-25	3.7E-27
R	36	4863.582775	0.000344	1.803E-25	4.8E-27
R	38	4864.578525	0.000392	1.454E-25	4.2E-27
R	40	4865.543055	0.000422	1.275E-25	3.7E-27
R	42	4866.475309	0.000545	1.063E-25	4.4E-27
R	44	4867.374703	0.000565	9.57E-26	3.9E-27
R	50	4869.867501	0.000573	8.78E-26	3.5E-27

Table 12: Line Positions and Intensities
for band 00031 ← 11102 of molecule 12C 16O2
Values corrected to 296K

	J''	Line Position (1/cm)	Position Uncertainty (1/cm)	Line Intensity (cm/molecule)	Intensity Uncertainty (cm/molecule)
P	35	4725.721489	0.002239	2.15E-26	2.8E-27
P	33	4727.581617	0.002053	2.39E-26	2.8E-27
P	32	4729.199506	0.001424	3.52E-26	2.8E-27
P	30	4730.946735	0.001353	3.79E-26	2.9E-27
P	27	4733.056995	0.001181	4.71E-26	3.1E-27
P	25	4734.844378	0.001015	5.42E-26	2.9E-27
P	24	4736.108959	0.001173	4.78E-26	3.2E-27
P	23	4736.615128	0.000995	5.64E-26	3.4E-27
P	22	4737.805934	0.000901	6.21E-26	3.0E-27
P	21	4738.368243	0.000970	5.87E-26	3.4E-27
P	20	4739.491559	0.000911	6.27E-26	3.4E-27
P	18	4741.164506	0.000760	7.59E-26	3.2E-27
P	17	4741.819043	0.000937	6.23E-26	3.4E-27
P	16	4742.826807	0.000790	7.41E-26	3.0E-27
P	14	4744.476922	0.000949	6.26E-26	3.1E-27
P	13	4745.200789	0.001013	5.91E-26	3.1E-27
P	12	4746.115345	0.000941	6.44E-26	3.4E-27
P	11	4746.862917	0.001052	5.80E-26	3.3E-27
P	10	4747.741794	0.001060	5.79E-26	3.4E-27
P	6	4750.961369	0.001923	3.18E-26	3.3E-27
P	5	4751.750351	0.002053	3.03E-26	3.3E-27
P	4	4752.555573	0.002016	3.12E-26	3.4E-27
R	7	4761.796534	0.001086	5.74E-26	3.2E-27
R	8	4762.626146	0.001239	5.01E-26	3.4E-27
R	10	4764.130230	0.000911	6.69E-26	3.2E-27
R	11	4764.735786	0.000856	7.05E-26	3.3E-27
R	12	4765.625539	0.000878	6.83E-26	3.2E-27
R	14	4767.105412	0.000808	7.36E-26	3.3E-27
R	15	4767.604353	0.000722	8.15E-26	3.2E-27
R	17	4769.011806	0.000827	6.99E-26	3.1E-27
R	18	4770.034578	0.000730	7.84E-26	3.1E-27
R	19	4770.398751	0.000719	7.93E-26	3.1E-27
R	20	4771.480212	0.000794	7.19E-26	3.5E-27
R	21	4771.769147	0.000881	6.40E-26	3.3E-27
R	22	4772.912837	0.000795	7.02E-26	3.0E-27
R	25	4774.452616	0.001037	5.37E-26	3.1E-27
R	26	4775.741682	0.000971	5.63E-26	3.1E-27
R	29	4777.062302	0.001472	3.46E-26	3.3E-27
R	30	4778.512231	0.001344	3.82E-26	3.0E-27

Table 13: Line Positions and Intensities
for band 31113 ← 11102 of molecule 12C 16O2
Values corrected to 296K

	J"	Line Position (1/cm)	Position Uncertainty (1/cm)	Line Intensity (cm/molecule)	Intensity Uncertainty (cm/molecule)
P	40	4894.568764	0.001460	3.44E-26	3.0E-27
P	38	4896.644591	0.001603	3.16E-26	3.1E-27
P	37	4897.129784	0.001126	4.84E-26	3.4E-27
P	36	4898.694414	0.000969	5.58E-26	3.2E-27
P	35	4899.225951	0.001013	5.23E-26	3.2E-27
P	34	4900.718467	0.000737	7.42E-26	3.2E-27
P	28	4906.632829	0.000445	1.306E-25	3.5E-27
P	27	4907.319308	0.000461	1.245E-25	3.3E-27
P	26	4908.550157	0.000462	1.253E-25	3.3E-27
P	24	4910.442813	0.000446	1.367E-25	4.1E-27
P	22	4912.312095	0.000423	1.414E-25	3.4E-27
P	21	4913.076170	0.000360	1.704E-25	3.7E-27
P	20	4914.145679	0.000284	2.235E-25	3.8E-27
P	13	4920.331102	0.000384	1.731E-25	3.9E-27
P	9	4923.772562	0.000395	1.879E-25	4.3E-27
P	6	4926.284954	0.000713	9.45E-26	3.6E-27
P	4	4927.919000	Fixed	6.17E-26	4.4E-27

Table 14: Position-related band constants
for band 40002 ← 01101 of molecule 12C 16O2
Values corrected to 296K

B' (1/cm)	3.901E-01
B' Uncertainty (1/cm)	1.828E-07
D' (1/cm)	8.905E-08
D' Uncertainty (1/cm)	3.627E-10
H' (1/cm)	5.661E-12
H' Uncertainty (1/cm)	1.519E-13
omega 01101 (unitless)	0.0192729
omega Uncertainty (unitless)	0.0000016

Table 15: Line Intensities
for band 40002 ← 01101 of molecule 12C 16O2
Values corrected to 296K

	J"	Line Intensity (cm/molecule)	Intensity Uncertainty (cm/molecule)
P	51	1.310E-26	Fixed
P	49	3.53E-26	4.1E-27
P	47	4.01E-26	3.1E-27
P	45	5.09E-26	3.3E-27
P	43	7.17E-26	3.6E-27
P	41	1.104E-25	3.6E-27
P	39	1.180E-25	Fixed
P	37	1.837E-25	5.4E-27
P	35	2.397E-25	5.0E-27
P	31	3.848E-25	5.3E-27
P	29	4.933E-25	4.9E-27
P	27	5.727E-25	4.7E-27
P	25	6.860E-25	5.4E-27
P	23	7.964E-25	6.5E-27
P	21	8.693E-25	5.0E-27
P	19	9.490E-25	5.2E-27
P	17	1.001E-24	7 E-27
P	15	9.00E-25	1.2E-26
P	13	8.831E-25	6.6E-27
P	11	6.973E-25	5.5E-27
P	9	5.681E-25	5.5E-27
P	7	3.152E-25	4.7E-27
P	5	1.268E-25	4.8E-27
P	3	3.140E-26	Fixed
R	1	1.810E-26	Fixed
R	3	1.222E-25	8.6E-27
R	5	3.210E-25	5.5E-27
R	7	5.254E-25	5.6E-27
R	9	8.147E-25	6.3E-27
R	11	9.330E-25	Fixed
R	15	1.204E-24	6 E-27
R	19	1.033E-24	6 E-27
R	21	9.550E-25	5.3E-27
R	23	8.691E-25	7.8E-27
R	25	7.107E-25	6.2E-27
R	27	6.222E-25	5.5E-27
R	29	5.239E-25	5.2E-27
R	33	3.344E-25	5.1E-27
R	35	2.672E-25	5.7E-27
R	43	9.30E-26	3.5E-27
R	45	7.28E-26	3.6E-27
R	47	1.000E-26	Fixed
R	49	1.910E-26	Fixed

Table 16: Position-related band constants
for band 20013 ← 00001 of molecule 13C 16O2
Values corrected to 296K

(G'-G'') (1/cm)	4748.062811
(G'-G'') Uncertainty (1/cm)	0.000174
B' (1/cm)	3.888E-01
B' Uncertainty (1/cm)	6.399E-06
B'' (1/cm)	3.902E-01
B'' Uncertainty (1/cm)	8.976E-06

Table 17: Line Intensities
for band 20013 ← 00001 of molecule 13C 16O2
Values corrected to 296K

	J"	Line Intensity (cm/molecule)	Intensity Uncertainty (cm/molecule)
P	54	3.03E-26	2.6E-27
P	52	3.10E-26	2.8E-27
P	50	4.38E-26	2.6E-27
P	48	6.09E-26	2.6E-27
P	46	8.42E-26	2.6E-27
P	40	1.905E-25	4.4E-27
P	38	2.389E-25	3.8E-27
P	36	2.931E-25	3.8E-27
P	34	3.718E-25	4.4E-27
P	32	4.504E-25	4.1E-27
P	30	5.297E-25	4.3E-27
P	28	6.233E-25	4.1E-27
P	26	7.123E-25	4.7E-27
P	24	7.910E-25	4.3E-27
P	22	8.637E-25	4.9E-27
P	20	9.274E-25	4.8E-27
P	18	9.604E-25	4.7E-27
P	16	9.739E-25	5.1E-27
P	14	9.433E-25	4.5E-27
P	12	9.062E-25	5.0E-27
P	10	8.124E-25	4.7E-27
P	8	7.021E-25	4.8E-27
P	6	5.564E-25	4.9E-27
P	4	6.912E-25	4.7E-27
P	2	2.025E-25	4.8E-27
R	0	1.114E-25	5.1E-27
R	2	2.980E-25	5.1E-27
R	4	4.965E-25	3.7E-27
R	6	6.618E-25	4.8E-27
R	8	7.686E-25	5.6E-27
R	10	9.217E-25	4.8E-27
R	12	9.969E-25	5.3E-27
R	14	1.041E-24	5 E-27
R	16	1.059E-24	5 E-27
R	18	1.036E-24	5 E-27
R	20	9.181E-25	5.7E-27
R	22	9.465E-25	5.4E-27
R	24	8.560E-25	4.9E-27
R	26	7.536E-25	5.4E-27
R	28	6.836E-25	5.1E-27
R	30	5.828E-25	4.9E-27
R	32	4.949E-25	4.5E-27
R	34	4.372E-25	5.1E-27
R	36	3.333E-25	4.4E-27
R	38	2.615E-25	5.2E-27
R	40	2.084E-25	4.2E-27
R	42	1.638E-25	5.0E-27
R	44	1.268E-25	3.9E-27
R	50	4.59E-26	2.9E-27

Table 18: Position- and intensity-related band constants for band 20013 ← 00001 of molecule 12C 16O2 Values corrected to 296K

(G'-G'') (1/cm)	4853.623217
(G'-G'') Uncertainty (1/cm)	0.0000013
A1 (unitless)	3.005E-04
A1 Uncertainty (unitless)	5.707E-06
A2 (unitless)	2.896E-05
A2 Uncertainty (unitless)	9.657E-08
A3 (unitless)	-3.250E-08
A3 Uncertainty (unitless)	2.691E-09
Sv/Qr (cm/molecule)	2.668E-23
Sv/Qr Uncertainty (cm/molecule)	7.272E-27

Table 19: Position- and intensity-related band constants for band 21113 ← 01101 of molecule 12C 16O2 Values corrected to 296K

(G'-G") (1/cm)	4807.694242
(G'-G") Uncertainty (1/cm)	0.000005
B' (1/cm)	3.894E-01
B' Uncertainty (1/cm)	1.528E-08
D' (1/cm)	1.757E-07
D' Uncertainty (1/cm)	9.331E-12
A2 (unitless)	2.281E-05
A2 Uncertainty (unitless)	2.310E-07
Sv/(Vo Qr) (cm/molecule)	6.678E-27
Sv/Qr Uncertainty (cm/molecule)	1.935E-30

Table 20: Position- and intensity-related band constants for band 20012 ← 00001 of molecule 13C 16O2 Values corrected to 296K

(G'-G'') (1/cm)	4887.384671
(G'-G'') Uncertainty (1/cm)	0.000006
B' (1/cm)	3.869E-01
B' Uncertainty (1/cm)	1.912E-08
D' (1/cm)	1.519E-07
D' Uncertainty (1/cm)	1.117E-11
A1 (unitless)	-2.572E-05
A1 Uncertainty (unitless)	5.331E-06
A2 (unitless)	1.571E-05
A2 Uncertainty (unitless)	2.657E-07
Sv/Qr (cm/molecule)	9.797E-25
Sv/Qr Uncertainty (cm/molecule)	3.341E-28

Table 21: Pressure-dependent self broadening and shift coefficients for band 20013 ← 00001 of molecule 12C 16O2 Values corrected to 296K

	J"	Line Position (1/cm)	Self Broadening (1/cm)/atm	Broadening Uncertainty (1/cm)/atm	Self Shift (1/cm)/atm	Self Shift Uncertainty (1/cm)/atm
P	80	4776.90	0.06130	2.60E-02	0.0000	Fixed
P	76	4781.55	0.05970	6.76E-03	-0.0103	6.89E-03
P	68	4790.56	0.06520	1.11E-03	-0.0120	1.13E-03
P	66	4792.75	0.06770	7.80E-04	-0.0083	7.67E-04
P	64	4794.92	0.06920	6.40E-04	-0.0094	6.02E-04
P	62	4797.06	0.07060	9.30E-04	-0.0077	8.64E-04
P	60	4799.18	0.06990	3.00E-04	-0.0078	2.54E-04
P	58	4801.27	0.07380	3.40E-04	-0.0076	2.84E-04
P	56	4803.34	0.07020	2.40E-04	-0.0073	1.86E-04
P	54	4805.40	0.07160	2.10E-04	-0.0076	1.55E-04
P	52	4807.43	0.07250	2.10E-04	-0.0071	1.73E-04
P	50	4809.43	0.07360	1.60E-04	-0.0074	1.23E-04
P	48	4811.42	0.07540	1.60E-04	-0.0075	1.41E-04
P	46	4813.39	0.07760	1.50E-04	-0.0074	1.42E-04
P	44	4815.34	0.07920	1.20E-04	-0.0076	1.53E-04
P	42	4817.26	0.08040	1.10E-04	-0.0070	1.56E-04
P	40	4819.17	0.08250	1.10E-04	-0.0076	1.83E-04
P	38	4821.06	0.08430	9.00E-05	-0.0069	1.73E-04
P	36	4822.93	0.08560	9.00E-05	-0.0060	1.75E-04
P	34	4824.78	0.08730	1.20E-04	-0.0069	2.33E-04
P	32	4826.61	0.08990	8.00E-05	-0.0057	1.90E-04
P	30	4828.43	0.09190	8.00E-05	-0.0051	2.07E-04
P	28	4830.23	0.09410	8.00E-05	-0.0057	2.07E-04
P	26	4832.01	0.09600	7.00E-05	-0.0051	2.02E-04
P	24	4833.77	0.09800	7.00E-05	-0.0054	2.06E-04
P	22	4835.52	0.10010	7.00E-05	-0.0052	2.13E-04
P	20	4837.24	0.10180	7.00E-05	-0.0054	2.05E-04
P	18	4838.96	0.10410	7.00E-05	-0.0074	2.03E-04
P	16	4840.65	0.10530	7.00E-05	-0.0062	2.05E-04
P	14	4842.33	0.10730	7.00E-05	-0.0074	2.09E-04
P	12	4843.99	0.10900	7.00E-05	-0.0071	2.08E-04
P	10	4845.64	0.11110	8.00E-05	-0.0073	2.08E-04
P	8	4847.27	0.11330	8.00E-05	-0.0078	2.06E-04
P	6	4848.88	0.11610	9.00E-05	-0.0080	2.07E-04
P	4	4850.48	0.11830	1.00E-04	-0.0087	1.93E-04
P	2	4852.06	0.12080	1.30E-04	-0.0077	1.70E-04
R	0	4854.40	0.12680	1.80E-04	-0.0023	1.60E-04
R	2	4855.94	0.11960	1.00E-04	-0.0008	1.83E-04
R	4	4857.46	0.11750	9.00E-05	-0.0011	2.04E-04
R	6	4858.97	0.11500	9.00E-05	-0.0018	2.22E-04
R	8	4860.46	0.11240	8.00E-05	-0.0035	2.14E-04
R	10	4861.94	0.11010	8.00E-05	-0.0036	2.15E-04
R	12	4863.40	0.10770	7.00E-05	-0.0041	2.15E-04
R	14	4864.84	0.10600	8.00E-05	-0.0048	2.20E-04
R	16	4866.27	0.10380	7.00E-05	-0.0065	2.11E-04
R	18	4867.67	0.10200	7.00E-05	-0.0064	2.07E-04
R	20	4869.06	0.10010	7.00E-05	-0.0065	2.11E-04
R	22	4870.44	0.09860	8.00E-05	-0.0077	2.20E-04
R	24	4871.79	0.09640	7.00E-05	-0.0080	2.08E-04
R	26	4873.13	0.09450	7.00E-05	-0.0088	2.06E-04
R	28	4874.45	0.09220	7.00E-05	-0.0089	2.06E-04
R	30	4875.75	0.09070	8.00E-05	-0.0089	2.16E-04
R	32	4877.03	0.08820	8.00E-05	-0.0097	1.93E-04
R	34	4878.29	0.08640	8.00E-05	-0.0099	1.83E-04
R	36	4879.54	0.08440	9.00E-05	-0.0098	1.86E-04
R	38	4880.76	0.08020	Fixed	-0.0111	1.83E-04
R	40	4881.96	0.08050	9.00E-05	-0.0096	1.57E-04
R	42	4883.15	0.07880	9.00E-05	-0.0097	1.47E-04

Band 20013 ← 00001 of molecule 12C 16O2 continues
Values corrected to 296K

	J"	Line Position (1/cm)	Self Broadening (1/cm)/atm	Broadening Uncertainty (1/cm)/atm	Self Shift (1/cm)/atm	Self Shift Uncertainty (1/cm)/atm
R	44	4884.31	0.07750	1.40E-04	-0.0093	1.76E-04
R	46	4885.45	0.07570	1.30E-04	-0.0093	1.42E-04
R	48	4886.57	0.07410	1.40E-04	-0.0090	1.28E-04
R	50	4887.66	0.07320	1.50E-04	-0.0087	1.25E-04
R	52	4888.74	0.07210	1.70E-04	-0.0085	1.29E-04
R	54	4889.79	0.07100	2.10E-04	-0.0079	1.58E-04
R	56	4890.82	0.06990	2.00E-04	-0.0084	1.51E-04
R	58	4891.82	0.06900	2.20E-04	-0.0080	1.82E-04
R	60	4892.80	0.06860	3.00E-04	-0.0078	2.61E-04
R	62	4893.76	0.06740	3.70E-04	-0.0082	3.47E-04
R	64	4894.69	0.06720	5.30E-04	-0.0088	4.97E-04
R	66	4895.59	0.07130	1.72E-03	-0.0207	1.49E-03
R	68	4896.47	0.06880	1.22E-03	-0.0081	1.26E-03
R	70	4897.32	0.06360	1.67E-03	-0.0091	1.73E-03
R	72	4898.15	0.06930	3.38E-03	-0.0135	3.43E-03
R	74	4898.94	0.06490	4.40E-03	-0.0082	4.40E-03

Table 22: Pressure-dependent self broadening and shift coefficients for band 20012 ← 00001 of molecule 12C 16O2 Values corrected to 296K

	J"	Line Position (1/cm)	Self Broadening (1/cm)/atm	Broadening Uncertainty (1/cm)/atm	Self Shift (1/cm)/atm	Self Shift Uncertainty (1/cm)/atm
P	68	4908.16	0.06630	7.40E-04	-0.0099	8.16E-04
P	66	4910.68	0.06640	3.40E-04	-0.0074	3.29E-04
P	64	4913.17	0.06260	2.70E-04	-0.0064	2.47E-04
P	62	4915.64	0.06810	2.20E-04	-0.0072	2.15E-04
P	60	4918.08	0.06680	2.00E-04	-0.0080	1.94E-04
P	58	4920.49	0.07040	2.20E-04	-0.0077	1.95E-04
P	56	4922.87	0.07220	2.00E-04	-0.0080	2.08E-04
P	54	4925.22	0.07360	2.10E-04	-0.0072	2.34E-04
P	52	4927.55	0.07510	2.00E-04	-0.0071	2.19E-04
P	50	4929.84	0.07860	2.10E-04	-0.0097	2.28E-04

Table 23: Pressure-dependent self broadening and shift coefficients for band 21113 ← 01101 of molecule 12C 16O2 Values corrected to 296K

	J"	Line Position (1/cm)	Self Broadening (1/cm)/atm	Broadening Uncertainty (1/cm)/atm	Self Shift (1/cm)/atm	Self Shift Uncertainty (1/cm)/atm
P	64	4749.79	0.05950	8.54E-03	-0.0094	8.56E-03
P	63	4748.32	0.06150	6.37E-03	-0.0388	6.38E-03
P	61	4750.50	0.07910	7.11E-03	-0.0164	6.93E-03
P	60	4753.94	0.05510	3.28E-03	-0.0045	3.30E-03
P	59	4752.69	0.07520	5.13E-03	-0.0113	4.89E-03
P	58	4755.98	0.06390	2.59E-03	-0.0112	2.62E-03
P	57	4754.85	0.07410	3.64E-03	-0.0090	3.55E-03
P	56	4758.00	0.06840	3.05E-03	-0.0092	3.06E-03
P	55	4756.99	0.06690	2.33E-03	-0.0142	2.23E-03
P	54	4760.00	0.07720	1.40E-03	-0.0096	1.41E-03
P	53	4759.11	0.07330	1.64E-03	-0.0077	1.60E-03
P	52	4761.98	0.07070	1.00E-03	-0.0102	9.93E-04
P	51	4761.21	0.07420	1.24E-03	-0.0056	9.16E-04
P	50	4763.95	0.06900	7.60E-04	-0.0100	7.74E-04
P	49	4763.29	0.07650	9.70E-04	-0.0059	7.08E-04
P	48	4765.89	0.07330	5.70E-04	-0.0074	5.68E-04
P	47	4765.34	0.07610	7.90E-04	-0.0060	5.75E-04
P	46	4767.82	0.07670	5.70E-04	-0.0073	5.49E-04
P	45	4767.37	0.07810	5.50E-04	-0.0067	4.08E-04
P	44	4769.73	0.07700	3.80E-04	-0.0068	3.61E-04
P	43	4769.38	0.07880	4.90E-04	-0.0072	3.57E-04
P	42	4771.62	0.07790	3.70E-04	-0.0077	3.89E-04
P	41	4771.37	0.07980	4.20E-04	-0.0075	3.33E-04
P	40	4773.50	0.07990	3.20E-04	-0.0076	2.90E-04
P	39	4773.34	0.08170	3.20E-04	-0.0069	2.38E-04
P	38	4775.35	0.08160	2.90E-04	-0.0075	2.55E-04
P	37	4775.28	0.08380	3.00E-04	-0.0064	2.35E-04
P	36	4777.20	0.08430	6.60E-04	-0.0046	6.23E-04
P	35	4777.21	0.09000	4.80E-04	-0.0106	4.34E-04
P	34	4779.02	0.08530	2.70E-04	-0.0062	2.35E-04
P	33	4779.12	0.08730	2.70E-04	-0.0066	2.00E-04
P	32	4780.83	0.08780	2.10E-04	-0.0061	1.69E-04
P	31	4781.00	0.08850	2.60E-04	-0.0062	1.97E-04
P	30	4782.62	0.09080	2.60E-04	-0.0073	1.90E-04
P	29	4782.86	0.09050	2.40E-04	-0.0060	1.77E-04
P	28	4784.40	0.09170	2.10E-04	-0.0058	1.57E-04
P	27	4784.71	0.09300	2.10E-04	-0.0060	1.55E-04
P	26	4786.16	0.09450	2.00E-04	-0.0058	1.50E-04
P	25	4786.53	0.09520	2.00E-04	-0.0058	1.48E-04
P	24	4787.91	0.09580	2.00E-04	-0.0056	1.43E-04
P	23	4788.34	0.09740	2.90E-04	-0.0052	2.35E-04
P	22	4789.64	0.09760	1.90E-04	-0.0055	1.39E-04
P	21	4790.13	0.09870	2.10E-04	-0.0056	1.50E-04
P	20	4791.35	0.09920	1.90E-04	-0.0055	1.41E-04
P	19	4791.89	0.10310	1.90E-04	-0.0080	1.45E-04
P	18	4793.05	0.10140	2.00E-04	-0.0053	1.46E-04
P	17	4793.64	0.10240	2.00E-04	-0.0056	1.48E-04
P	16	4794.74	0.10300	2.00E-04	-0.0052	1.49E-04
P	15	4795.37	0.10350	1.90E-04	-0.0052	1.45E-04
P	14	4796.41	0.10460	3.20E-04	-0.0044	2.44E-04
P	13	4797.08	0.10590	2.40E-04	-0.0052	1.89E-04
P	12	4798.06	0.10670	2.20E-04	-0.0054	1.54E-04
P	11	4798.77	0.10770	2.10E-04	-0.0047	1.54E-04
P	10	4799.71	0.10830	2.20E-04	-0.0059	1.65E-04
P	9	4800.44	0.11050	2.60E-04	-0.0046	1.95E-04
P	8	4801.33	0.11140	2.40E-04	-0.0045	1.82E-04
P	7	4802.09	0.11330	2.30E-04	-0.0045	1.74E-04
P	6	4802.94	0.11530	2.40E-04	-0.0047	1.92E-04

Band 21113 ← 01101 of molecule 12C 16O2 continues
Values corrected to 296K

	J"	Line Position (1/cm)	Self Broadening (1/cm)/atm	Broadening Uncertainty (1/cm)/atm	Self Shift (1/cm)/atm	Self Shift Uncertainty (1/cm)/atm
P	5	4803.72	0.11790	3.00E-04	-0.0046	2.25E-04
P	4	4804.54	0.12100	2.80E-04	-0.0040	2.33E-04
P	3	4805.33	0.12260	4.90E-04	-0.0031	3.53E-04
P	2	4806.13	0.12730	5.20E-04	-0.0029	4.87E-04
R	1	4809.24	0.12390	8.00E-04	-0.0039	5.79E-04
R	2	4810.02	0.12410	3.30E-04	-0.0026	2.91E-04
R	3	4810.76	0.11920	3.10E-04	-0.0022	2.28E-04
R	4	4811.55	0.11770	3.00E-04	-0.0032	2.46E-04
R	5	4812.25	0.11530	2.60E-04	-0.0032	1.97E-04
R	6	4813.07	0.11330	2.50E-04	-0.0032	1.88E-04
R	7	4813.72	0.11190	2.30E-04	-0.0035	1.74E-04
R	8	4814.57	0.11020	2.20E-04	-0.0038	1.66E-04
R	9	4815.18	0.10860	2.70E-04	-0.0037	1.98E-04
R	10	4816.06	0.10750	2.30E-04	-0.0046	1.62E-04
R	11	4816.61	0.10640	2.10E-04	-0.0047	1.56E-04
R	12	4817.53	0.10360	5.20E-04	-0.0072	5.58E-04
R	13	4818.02	0.10450	2.00E-04	-0.0051	1.52E-04
R	14	4818.99	0.10260	2.50E-04	-0.0044	1.86E-04
R	15	4819.42	0.10260	2.30E-04	-0.0055	1.77E-04
R	16	4820.43	0.10190	2.00E-04	-0.0047	1.54E-04
R	17	4820.79	0.10030	2.40E-04	-0.0056	1.82E-04
R	18	4821.86	0.10030	2.00E-04	-0.0052	1.54E-04
R	19	4822.15	0.09720	2.30E-04	-0.0043	2.26E-04
R	20	4823.27	0.09860	2.30E-04	-0.0054	1.78E-04
R	21	4823.48	0.09690	2.20E-04	-0.0066	1.70E-04
R	22	4824.67	0.09450	3.50E-04	-0.0051	2.42E-04
R	23	4824.80	0.10100	8.30E-04	-0.0094	7.53E-04
R	24	4826.05	0.09210	3.00E-04	-0.0078	2.14E-04
R	25	4826.10	0.09580	3.00E-04	-0.0087	2.30E-04
R	26	4827.41	0.09090	3.00E-04	-0.0058	2.19E-04
R	27	4827.37	0.09520	3.10E-04	-0.0049	2.38E-04
R	28	4828.76	0.09130	2.60E-04	-0.0068	2.01E-04
R	29	4828.63	0.09010	3.10E-04	-0.0063	2.38E-04
R	30	4830.09	0.08810	3.60E-04	-0.0069	2.73E-04
R	31	4829.86	0.08740	3.00E-04	-0.0067	2.25E-04
R	32	4831.41	0.08710	2.50E-04	-0.0076	1.93E-04
R	33	4831.07	0.08670	2.60E-04	-0.0071	1.98E-04
R	34	4832.71	0.08560	2.60E-04	-0.0076	2.04E-04
R	35	4832.26	0.08450	3.60E-04	-0.0074	2.78E-04
R	36	4833.99	0.08370	3.60E-04	-0.0076	2.99E-04
R	37	4833.43	0.08090	3.70E-04	-0.0081	2.92E-04
R	38	4835.25	0.08220	3.80E-04	-0.0076	3.23E-04
R	39	4834.58	0.08140	3.60E-04	-0.0080	2.77E-04
R	40	4836.49	0.08150	3.40E-04	-0.0083	2.99E-04
R	41	4835.71	0.07610	6.40E-04	-0.0095	4.77E-04
R	42	4837.72	0.08040	4.40E-04	-0.0079	4.01E-04
R	43	4836.81	0.07870	6.00E-04	-0.0076	4.72E-04
R	45	4837.89	0.07790	6.90E-04	-0.0070	5.40E-04
R	46	4840.11	0.07860	6.20E-04	-0.0099	6.04E-04
R	48	4841.28	0.07720	7.40E-04	-0.0080	7.28E-04
R	49	4839.98	0.07870	1.21E-03	-0.0049	9.37E-04
R	50	4842.43	0.08000	2.49E-03	-0.0171	2.46E-03
R	51	4840.99	0.07190	1.86E-03	-0.0059	2.31E-03
R	52	4843.56	0.07680	1.47E-03	-0.0114	1.52E-03
R	53	4841.98	0.07830	3.14E-03	-0.0119	3.46E-03
R	54	4844.67	0.07530	1.75E-03	-0.0095	1.76E-03
R	56	4845.76	0.07590	4.92E-03	-0.0171	4.91E-03
R	58	4846.83	0.07720	3.95E-03	-0.0216	4.01E-03

Table 24: Pressure-dependent self broadening and shift coefficients for band 40002 ← 01101 of molecule 12C 16O2 Values corrected to 296K

	J"	Line Position (1/cm)	Self Broadening (1/cm)/atm	Broadening Uncertainty (1/cm)/atm	Self Shift (1/cm)/atm	Self Shift Uncertainty (1/cm)/atm
P	37	4778.80	0.08180	4.00E-03	0.0044	2.75E-03
P	35	4780.42	0.08570	2.98E-03	0.0022	2.12E-03
P	31	4783.64	0.08690	1.84E-03	-0.0027	1.34E-03
P	29	4785.25	0.09310	1.59E-03	-0.0070	1.17E-03
P	27	4786.86	0.09170	1.28E-03	-0.0046	9.34E-04
P	25	4788.46	0.09690	1.32E-03	-0.0063	9.84E-04
P	23	4790.06	0.09860	1.43E-03	-0.0062	1.02E-03
P	21	4791.66	0.09590	9.70E-04	-0.0071	7.19E-04
P	19	4793.25	0.09980	9.70E-04	-0.0050	7.21E-04
P	17	4794.84	0.10340	1.25E-03	-0.0027	9.30E-04
P	15	4796.42	0.10560	3.30E-03	-0.0037	2.82E-03
P	13	4798.00	0.10420	1.42E-03	0.0065	9.94E-04
P	11	4799.57	0.10990	1.51E-03	0.0032	1.10E-03
P	9	4801.14	0.10820	1.78E-03	0.0051	1.28E-03
P	7	4802.71	0.10300	2.64E-03	0.0059	1.85E-03
P	5	4804.27	0.09020	5.62E-03	0.0085	3.99E-03
R	3	4811.30	0.11910	1.15E-02	0.0311	9.01E-03
R	5	4812.86	0.11360	3.20E-03	0.0115	2.25E-03
R	7	4814.42	0.10410	1.92E-03	0.0015	1.38E-03
R	9	4815.98	0.11100	1.56E-03	0.0089	1.09E-03
R	15	4820.62	0.10430	9.60E-04	0.0056	7.39E-04
R	19	4823.68	0.09510	1.21E-03	-0.0087	9.50E-04
R	21	4825.21	0.09440	9.60E-04	-0.0067	7.33E-04
R	23	4826.73	0.09570	1.74E-03	-0.0075	1.26E-03
R	25	4828.24	0.08600	1.58E-03	-0.0063	1.15E-03
R	27	4829.76	0.09060	1.54E-03	-0.0051	1.16E-03
R	29	4831.27	0.08940	1.69E-03	-0.0016	1.28E-03
R	33	4834.28	0.08580	2.54E-03	0.0051	1.91E-03
R	35	4835.78	0.07590	3.47E-03	0.0137	2.59E-03

Table 25: Pressure-dependent self broadening and shift coefficients for band 21112 ← 01101 of molecule 12C 16O2 Values corrected to 296K

	J"	Line Position (1/cm)	Self Broadening (1/cm)/atm	Broadening Uncertainty (1/cm)/atm	Self Shift (1/cm)/atm	Self Shift Uncertainty (1/cm)/atm
P	57	4909.41	0.07250	1.34E-03	-0.0025	1.40E-03
P	58	4909.74	0.06790	1.08E-03	0.0013	1.08E-03
P	55	4911.77	0.07210	1.09E-03	-0.0086	1.12E-03
P	56	4912.01	0.07170	1.01E-03	-0.0045	1.01E-03
P	53	4914.09	0.07060	Fixed	-0.0063	6.17E-04
P	54	4914.25	0.07150	7.30E-04	-0.0091	7.22E-04
P	51	4916.39	0.07450	6.30E-04	-0.0090	6.41E-04
P	52	4916.46	0.07380	6.10E-04	-0.0075	6.50E-04
P	50	4918.65	0.07590	9.70E-04	0.0028	9.99E-04
P	49	4918.66	0.07490	6.70E-04	-0.0120	6.99E-04
P	48	4920.81	0.07690	3.60E-04	-0.0075	3.69E-04
P	47	4920.90	0.07670	3.20E-04	-0.0074	3.25E-04
P	46	4922.95	0.07640	3.80E-04	-0.0080	4.16E-04
P	45	4923.11	0.07670	2.80E-04	-0.0073	2.85E-04
P	44	4925.07	0.07790	2.80E-04	-0.0061	3.02E-04
P	43	4925.30	0.07890	3.50E-04	-0.0066	3.59E-04
P	42	4927.16	0.07770	2.80E-04	-0.0082	2.83E-04
P	41	4927.45	0.07990	3.30E-04	-0.0061	3.27E-04
P	40	4929.23	0.08120	2.30E-04	-0.0070	2.27E-04
P	39	4929.58	0.08100	2.20E-04	-0.0065	2.19E-04

Table 26: Pressure-dependent self broadening and shift coefficients for band 22213 ← 02201 of molecule 12C 16O2 Values corrected to 296K

	J"	Line Position (1/cm)	Self Broadening (1/cm)/atm	Broadening Uncertainty (1/cm)/atm	Self Shift (1/cm)/atm	Self Shift Uncertainty (1/cm)/atm
P	39	4734.64	0.08300	5.52E-03	-0.0074	5.25E-03
P	37	4736.55	0.08980	4.54E-03	-0.0059	4.35E-03
P	35	4738.45	0.09100	4.55E-03	-0.0113	4.47E-03
P	32	4741.28	0.08930	2.88E-03	0.0036	2.03E-03
P	31	4742.17	0.09310	2.63E-03	-0.0084	2.53E-03
P	30	4743.12	0.09320	2.75E-03	-0.0057	2.54E-03
P	29	4744.01	0.09570	2.35E-03	-0.0069	2.25E-03
P	27	4745.82	0.09540	2.08E-03	-0.0041	1.98E-03
P	26	4746.74	0.09530	2.01E-03	-0.0043	1.91E-03
P	25	4747.62	0.09630	1.96E-03	-0.0038	1.92E-03
P	24	4748.52	0.09930	1.89E-03	-0.0055	1.80E-03
P	23	4749.40	0.09740	1.89E-03	-0.0050	1.85E-03
P	22	4750.29	0.09840	1.84E-03	-0.0100	1.78E-03
P	21	4751.16	0.09950	1.74E-03	-0.0042	1.67E-03
P	20	4752.04	0.09980	1.71E-03	-0.0050	1.65E-03
P	19	4752.90	0.10130	1.57E-03	-0.0056	1.47E-03
P	18	4753.77	0.10590	1.68E-03	-0.0035	1.58E-03
P	17	4754.62	0.10560	1.65E-03	-0.0059	1.55E-03
P	16	4755.48	0.10620	1.71E-03	-0.0043	1.65E-03
P	15	4756.33	0.10640	1.77E-03	-0.0064	1.72E-03
P	14	4757.18	0.10450	1.76E-03	-0.0036	1.66E-03
P	12	4758.86	0.10820	1.98E-03	-0.0051	1.94E-03
P	11	4759.69	0.10930	2.03E-03	-0.0028	1.90E-03
P	9	4761.34	0.11280	2.41E-03	-0.0065	2.27E-03
P	8	4762.16	0.11700	2.86E-03	-0.0111	2.74E-03
P	7	4762.97	0.12450	3.18E-03	-0.0032	2.94E-03
P	6	4763.79	0.12410	6.65E-03	-0.0379	5.58E-03
P	4	4765.39	0.13260	7.69E-03	0.0125	7.41E-03
R	4	4772.40	0.12510	5.02E-03	0.0073	4.93E-03
R	6	4773.91	0.11450	3.21E-03	-0.0133	3.14E-03
R	7	4774.66	0.11500	2.62E-03	-0.0037	2.47E-03
R	10	4776.87	0.11020	1.93E-03	-0.0056	2.06E-03
R	12	4778.33	0.10350	1.68E-03	-0.0059	1.58E-03
R	14	4779.76	0.10810	1.72E-03	-0.0048	1.67E-03
R	15	4780.47	0.10280	1.86E-03	-0.0073	1.80E-03
R	16	4781.18	0.10270	1.69E-03	-0.0034	1.69E-03
R	17	4781.88	0.10230	1.54E-03	-0.0037	1.46E-03
R	19	4783.27	0.10240	1.53E-03	-0.0042	1.45E-03
R	20	4783.96	0.10030	1.57E-03	-0.0047	1.50E-03
R	21	4784.64	0.10530	2.17E-03	-0.0057	2.25E-03
R	22	4785.32	0.09790	1.70E-03	-0.0046	1.69E-03
R	24	4786.67	0.09720	2.00E-03	-0.0047	2.06E-03
R	25	4787.32	0.09620	1.85E-03	-0.0060	1.78E-03
R	26	4788.00	0.09590	2.39E-03	-0.0032	2.54E-03
R	27	4788.63	0.09840	2.16E-03	-0.0072	2.10E-03
R	28	4789.31	0.09280	2.12E-03	-0.0060	2.05E-03
R	29	4789.92	0.08880	2.42E-03	-0.0082	2.45E-03
R	31	4791.20	0.08490	2.72E-03	-0.0103	2.81E-03
R	33	4792.45	0.08500	2.82E-03	-0.0065	2.76E-03

Table 27: Pressure-dependent self broadening and shift coefficients for band 20013 ← 00001 of molecule 13C 16O2
Values corrected to 296K

	J"	Line Position (1/cm)	Self Broadening (1/cm)/atm	Broadening Uncertainty (1/cm)/atm	Self Shift (1/cm)/atm	Self Shift Uncertainty (1/cm)/atm
P	40	4714.59	0.07740	2.80E-03	-0.0061	2.63E-03
P	38	4716.38	0.07690	2.11E-03	-0.0076	2.04E-03
P	36	4718.16	0.07780	1.76E-03	-0.0059	1.70E-03
P	34	4719.92	0.08270	1.58E-03	-0.0055	1.51E-03
P	32	4721.68	0.08540	1.34E-03	-0.0058	1.26E-03
P	30	4723.42	0.08730	1.19E-03	-0.0053	1.12E-03
P	28	4725.14	0.08970	1.03E-03	-0.0059	9.73E-04
P	26	4726.85	0.09210	9.60E-04	-0.0062	9.31E-04
P	24	4728.56	0.09370	8.70E-04	-0.0047	8.26E-04
P	22	4730.24	0.09580	8.70E-04	-0.0052	8.22E-04
P	20	4731.92	0.09760	8.30E-04	-0.0059	7.85E-04
P	18	4733.59	0.09970	8.10E-04	-0.0049	7.60E-04
P	16	4735.24	0.10080	8.30E-04	-0.0049	7.81E-04
P	14	4736.88	0.10190	8.20E-04	-0.0055	7.76E-04
P	12	4738.51	0.10470	9.50E-04	-0.0057	9.08E-04
P	10	4740.13	0.10730	1.02E-03	-0.0031	9.60E-04
P	8	4741.74	0.10920	1.20E-03	-0.0043	1.13E-03
P	6	4743.34	0.11430	1.62E-03	-0.0131	1.42E-03
P	4	4744.92	0.12390	1.39E-03	0.0192	1.17E-03
P	2	4746.50	0.12110	4.59E-03	-0.0266	3.31E-03
R	0	4748.84	0.14090	1.01E-02	-0.0183	7.16E-03
R	2	4750.39	0.11780	3.20E-03	-0.0165	2.52E-03
R	4	4751.92	0.11650	Fixed	-0.0110	1.63E-03
R	6	4753.44	0.11230	1.34E-03	0.0030	1.21E-03
R	8	4754.96	0.11020	1.22E-03	-0.0041	1.14E-03
R	10	4756.46	0.10620	9.10E-04	-0.0035	8.68E-04
R	12	4757.95	0.10520	9.40E-04	-0.0067	9.87E-04
R	14	4759.43	0.10070	7.50E-04	-0.0050	7.05E-04
R	16	4760.90	0.09960	7.40E-04	-0.0045	6.93E-04
R	18	4762.35	0.09740	7.50E-04	-0.0049	6.99E-04
R	20	4763.79	0.09250	1.33E-03	-0.0005	1.48E-03
R	22	4765.22	0.09490	8.50E-04	-0.0070	8.12E-04
R	24	4766.64	0.09320	8.50E-04	-0.0056	8.25E-04
R	26	4768.05	0.08980	9.80E-04	-0.0056	9.17E-04
R	28	4769.44	0.08990	1.12E-03	-0.0048	1.12E-03
R	30	4770.81	0.08680	1.17E-03	-0.0059	1.12E-03
R	32	4772.18	0.08480	1.29E-03	-0.0072	1.25E-03
R	34	4773.52	0.09040	1.96E-03	-0.0063	2.07E-03
R	36	4774.86	0.08390	1.87E-03	-0.0056	1.82E-03
R	38	4776.18	0.07800	2.42E-03	-0.0051	2.41E-03
R	40	4777.48	0.07570	2.64E-03	-0.0027	2.57E-03
R	42	4778.77	0.07510	3.62E-03	-0.0076	3.62E-03
R	44	4780.04	0.07740	4.14E-03	-0.0056	3.95E-03
R	46	4781.30	0.07070	4.29E-03	-0.0100	3.89E-03

Table 28: Pressure-dependent self broadening and shift coefficients for band 20012 ← 00001 of molecule 13C 16O2 Values corrected to 296K

	J"	Line Position (1/cm)	Self Broadening (1/cm)/atm	Broadening Uncertainty (1/cm)/atm	Self Shift (1/cm)/atm	Self Shift Uncertainty (1/cm)/atm
P	52	4837.79	0.06760	1.84E-03	-0.0075	1.84E-03
P	50	4840.04	0.06890	1.32E-03	-0.0101	1.31E-03
P	46	4844.46	0.07240	8.00E-04	-0.0064	7.71E-04
P	44	4846.63	0.07300	6.40E-04	-0.0069	6.33E-04
P	42	4848.77	0.07670	9.00E-04	-0.0064	8.30E-04
P	40	4850.88	0.07800	4.10E-04	-0.0061	3.67E-04
P	38	4852.97	0.07960	3.00E-04	-0.0048	2.59E-04
P	36	4855.02	0.08180	2.80E-04	-0.0059	2.32E-04
P	34	4857.05	0.08420	3.10E-04	-0.0054	2.57E-04
P	32	4859.05	0.08830	6.80E-04	-0.0051	5.73E-04
P	30	4861.03	0.08950	2.90E-04	-0.0054	2.29E-04
P	28	4862.98	0.09140	2.90E-04	-0.0057	2.33E-04
P	26	4864.90	0.09020	8.20E-04	-0.0059	6.61E-04
P	24	4866.79	0.09520	2.80E-04	-0.0050	2.11E-04
P	22	4868.65	0.09750	2.80E-04	-0.0051	2.14E-04
P	20	4870.49	0.09620	7.00E-04	-0.0059	5.40E-04
P	18	4872.30	0.10020	2.60E-04	-0.0048	1.99E-04
P	16	4874.09	0.10190	2.70E-04	-0.0050	2.06E-04
P	14	4875.84	0.10170	4.20E-04	-0.0055	3.22E-04
P	12	4877.57	0.10420	2.50E-04	-0.0047	1.87E-04
P	10	4879.28	0.10670	2.90E-04	-0.0045	2.22E-04
P	8	4880.95	0.10970	3.00E-04	-0.0042	2.41E-04
P	6	4882.60	0.11150	2.90E-04	-0.0036	2.40E-04
P	4	4884.22	0.11360	4.40E-04	-0.0036	3.63E-04
P	2	4885.82	0.11950	4.80E-04	-0.0031	4.37E-04
R	0	4888.16	0.12700	8.60E-04	-0.0017	8.48E-04
R	2	4889.69	0.11460	4.20E-04	-0.0031	3.73E-04
R	4	4891.19	0.11300	2.60E-04	-0.0026	2.15E-04
R	6	4892.66	0.10970	2.50E-04	-0.0028	2.03E-04
R	8	4894.10	0.10790	2.30E-04	-0.0032	1.76E-04
R	10	4895.52	0.10510	2.40E-04	-0.0037	1.77E-04
R	12	4896.91	0.10350	2.20E-04	-0.0036	1.57E-04
R	14	4898.28	0.10140	2.10E-04	-0.0041	1.53E-04
R	16	4899.61	0.09880	2.40E-04	-0.0048	1.65E-04
R	18	4900.92	0.09750	2.10E-04	-0.0046	1.51E-04
R	20	4902.20	0.09600	1.90E-04	-0.0054	1.44E-04
R	22	4903.46	0.09450	2.00E-04	-0.0055	1.50E-04
R	24	4904.68	0.09300	2.00E-04	-0.0063	1.50E-04
R	26	4905.88	0.09050	2.00E-04	-0.0060	1.50E-04
R	28	4907.05	0.08990	2.20E-04	-0.0077	1.70E-04
R	30	4908.19	0.08650	2.50E-04	-0.0064	1.97E-04
R	32	4909.30	0.08560	2.30E-04	-0.0060	1.84E-04
R	34	4910.39	0.08100	3.10E-04	-0.0086	3.02E-04
R	36	4911.45	0.08220	2.50E-04	-0.0065	2.10E-04
R	38	4912.47	0.07870	3.10E-04	-0.0083	2.68E-04
R	40	4913.47	0.07910	3.20E-04	-0.0069	2.83E-04
R	42	4914.44	0.07720	4.50E-04	-0.0081	4.16E-04
R	44	4915.38	0.07710	4.50E-04	-0.0069	4.27E-04
R	46	4916.30	0.07510	6.40E-04	-0.0090	6.25E-04
R	48	4917.18	0.07940	7.50E-04	-0.0126	7.41E-04
R	50	4918.03	0.07480	1.37E-03	-0.0101	1.32E-03
R	54	4919.65	0.07190	1.79E-03	-0.0066	1.81E-03
R	56	4920.41	0.06800	4.50E-03	-0.0146	3.54E-03

Figure 17: A comparison of self-broadening coefficients between this work and the 2000 HITRAN line list

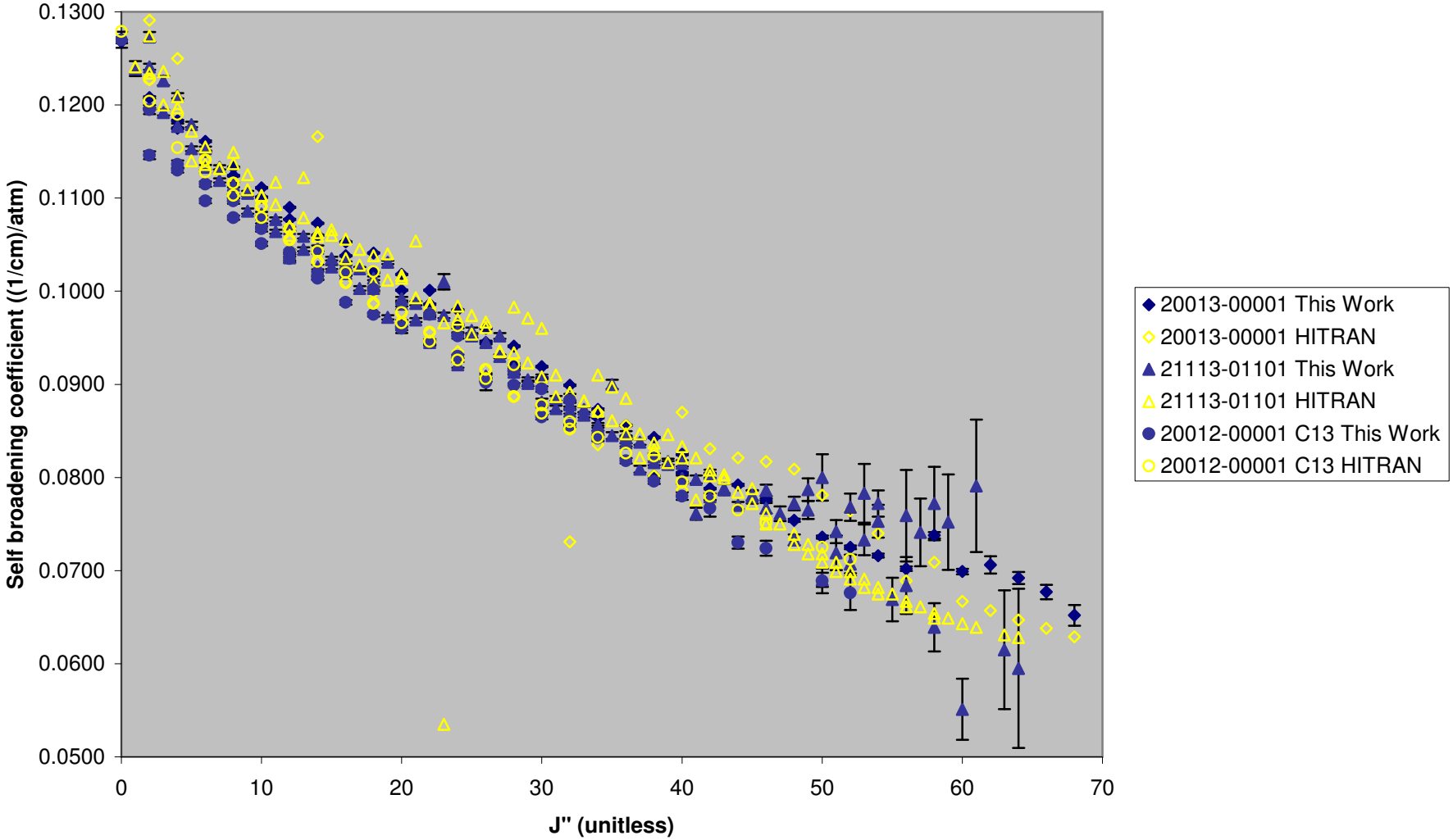

Figure 18: Self broadening coefficient as a function of |m|

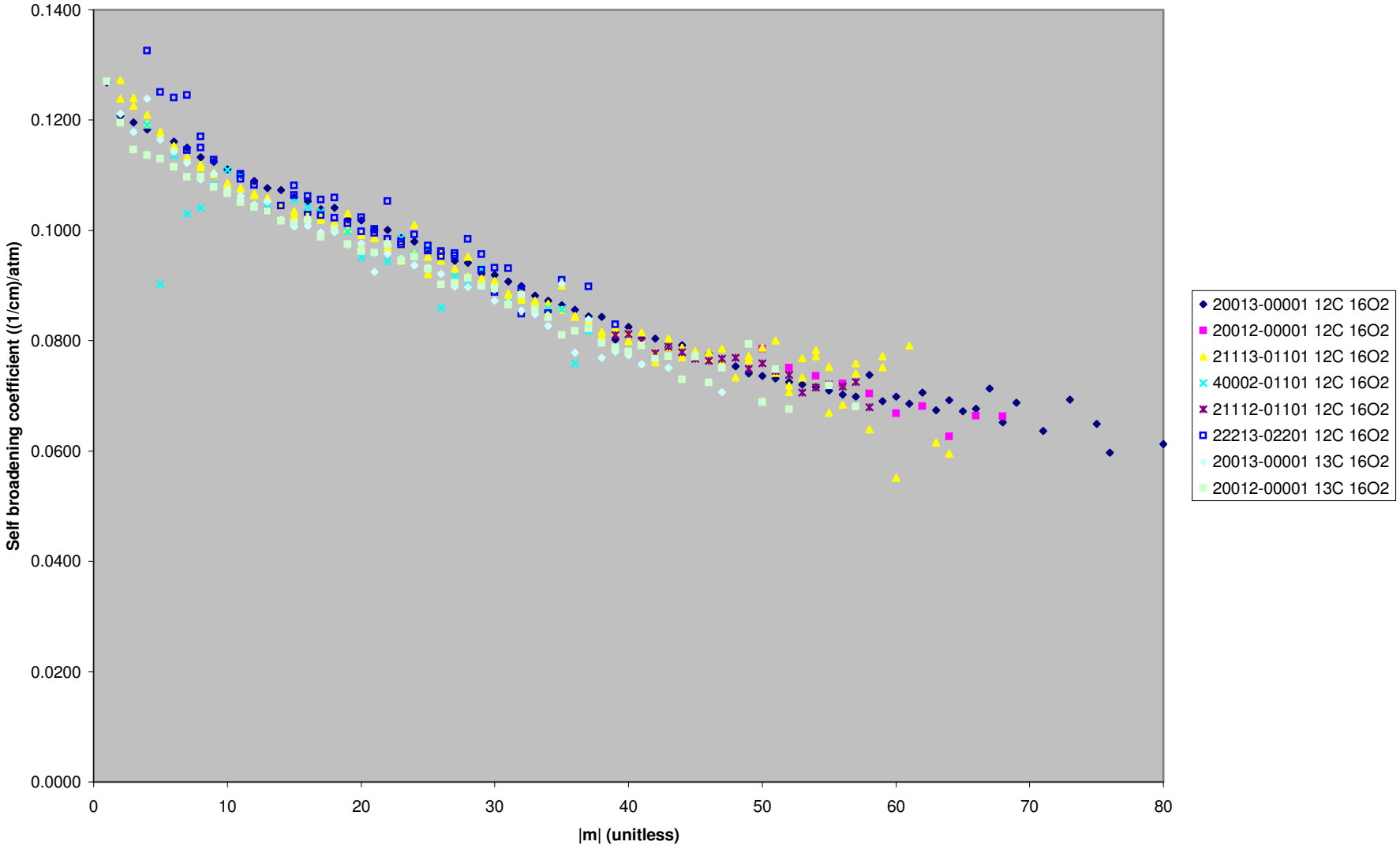

Figure 19: Self broadening coefficient as a function of |m|

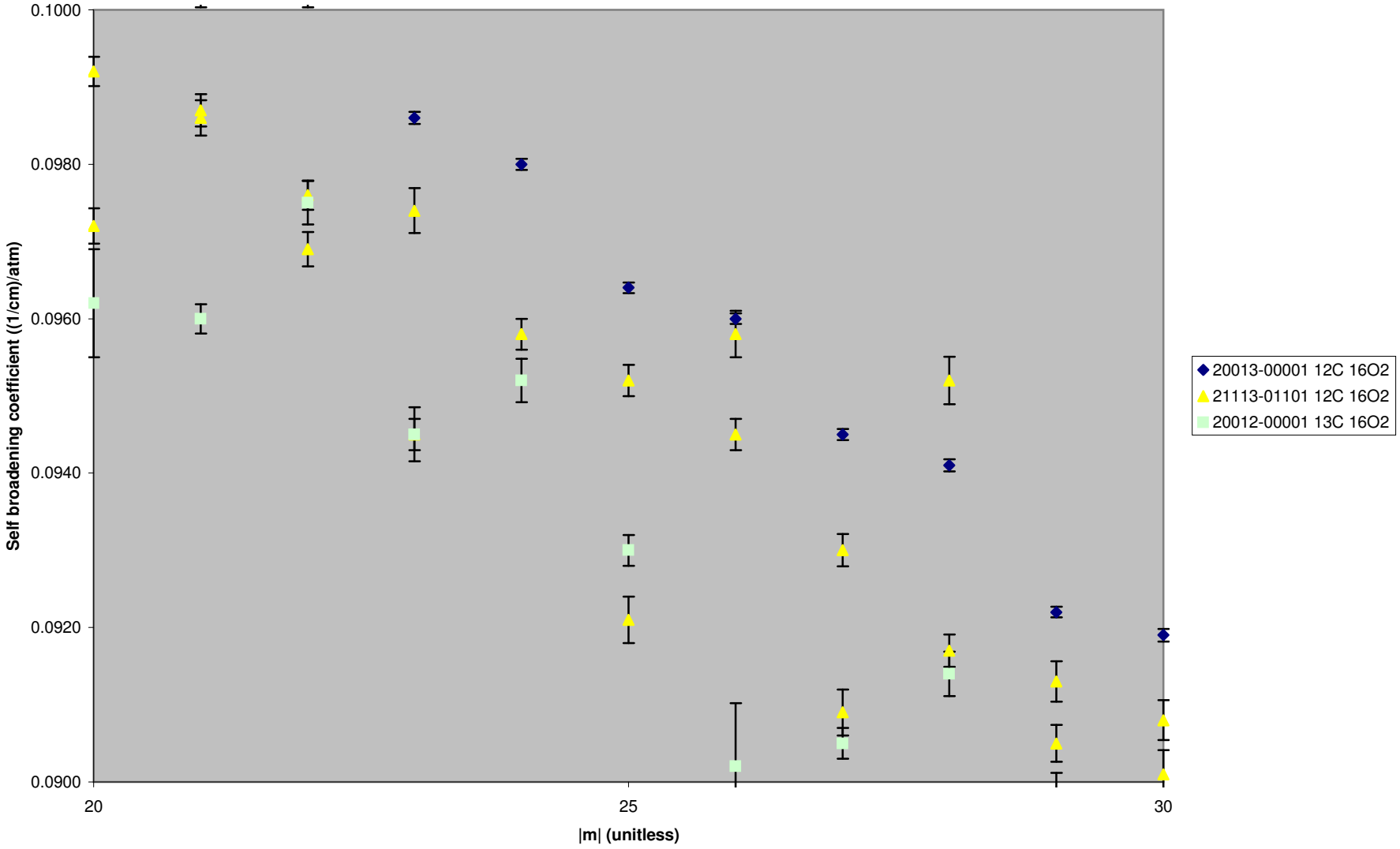

Figure 20: Self shift coefficient as a function of wavenumber

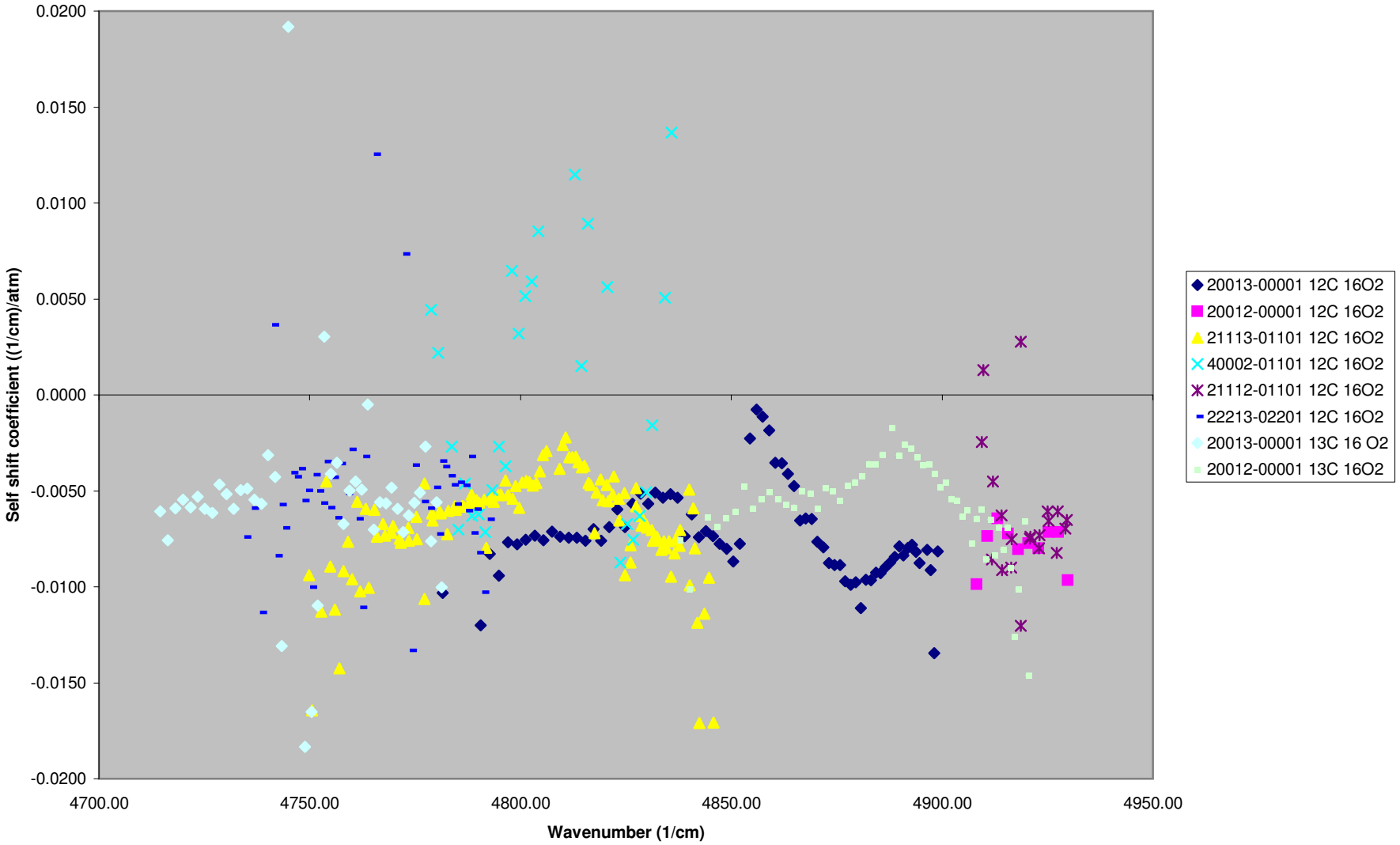

Figure 21: Self shift coefficient as a function of wavenumber

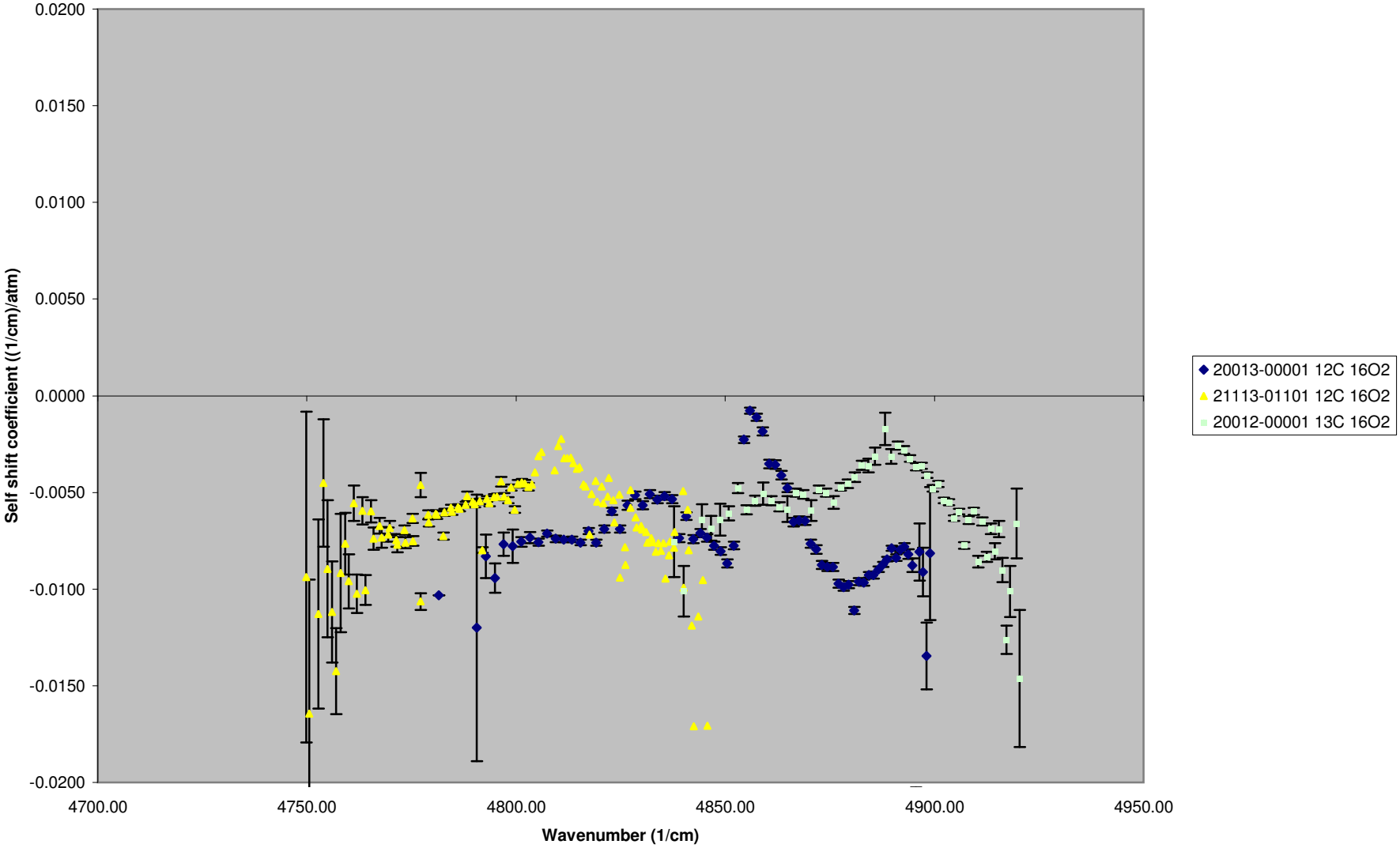

Figure 22: Self shift coefficient as a function of wavenumber

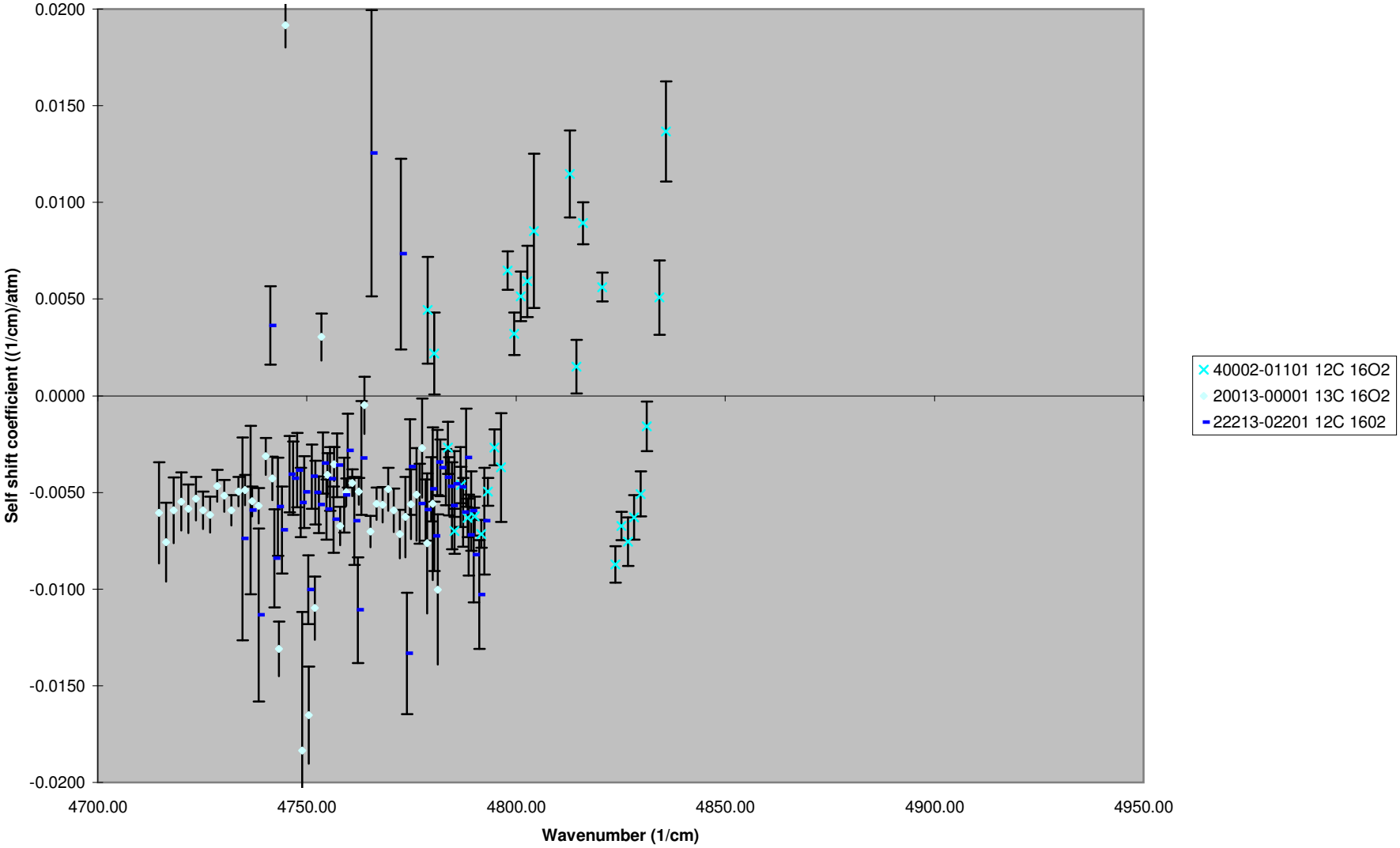

Figure 23: Self shift coefficient as a function of m

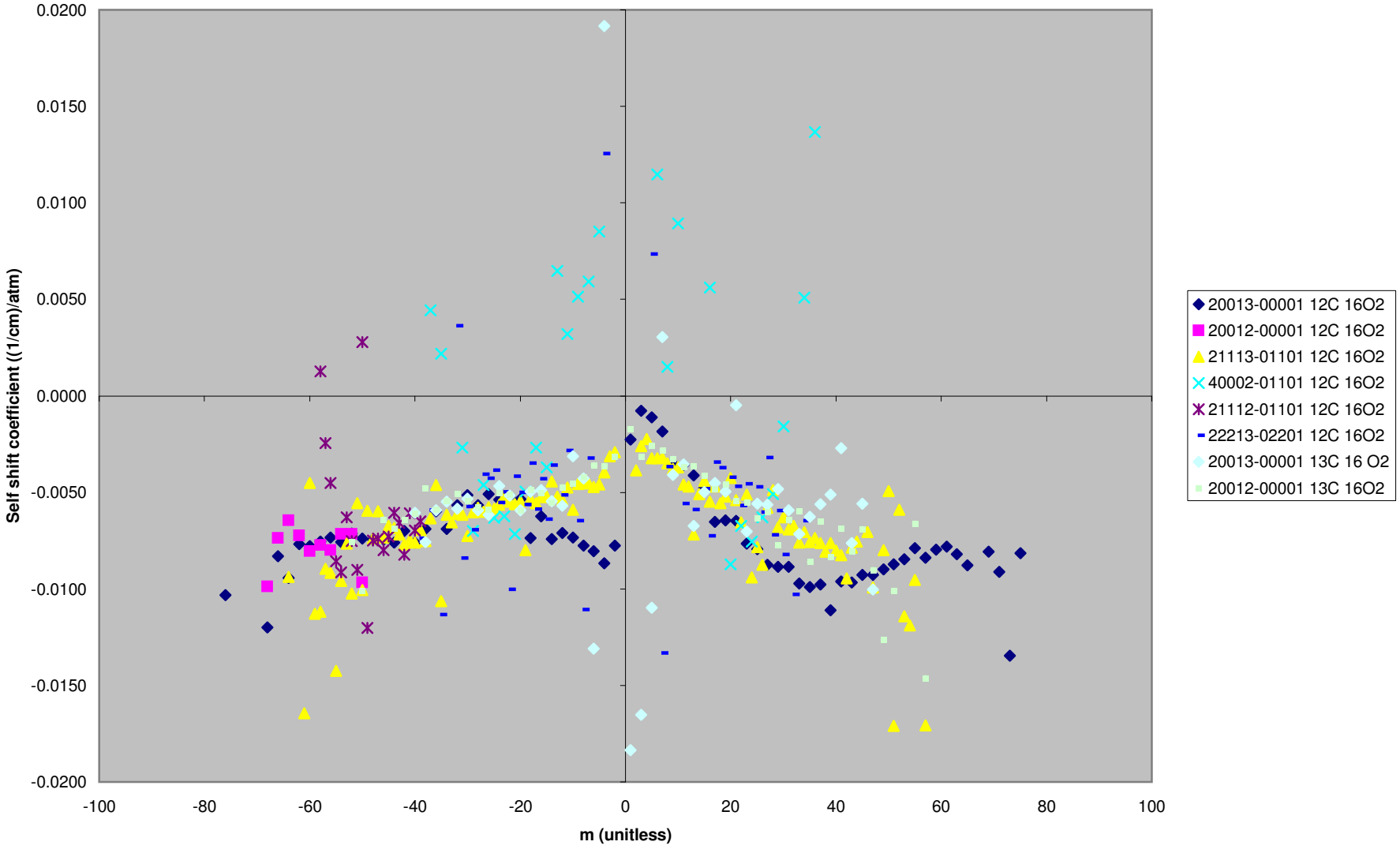

Figure 24: Self shift coefficient as a function of m

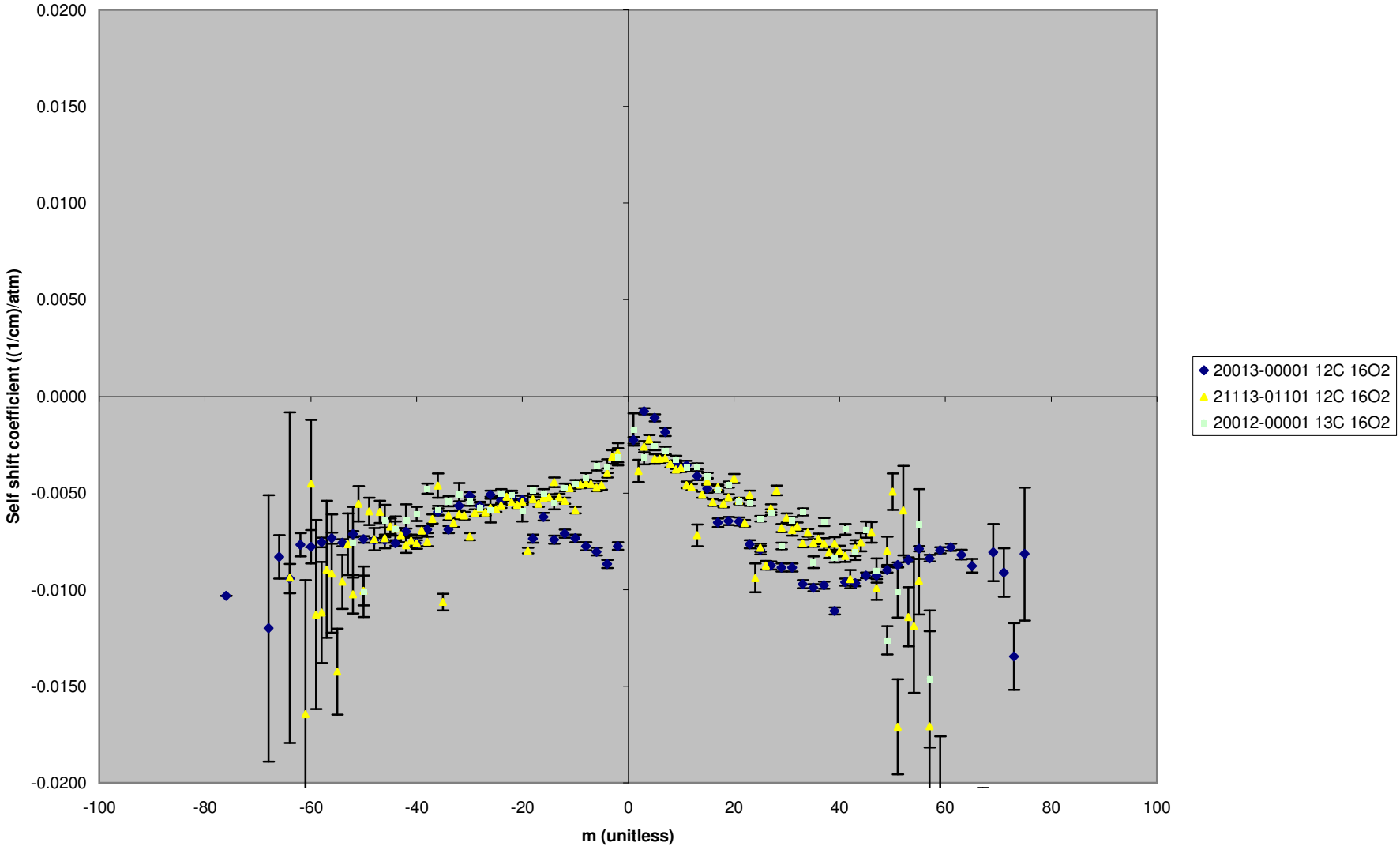

Figure 25: Self shift coefficient as a function of m